Diffusion Weighted Magnetic Resonance Imaging in the Differentiation between Benign and

Metastatic Lymph Nodes in Canine Patients with Head and Neck Disease

Jessica Anne Stahle

Thesis submitted to the faculty of the Virginia Polytechnic Institute and State University in

partial fulfillment of the requirements for the degree of

Master of Science

In

Biomedical and Veterinary Sciences

Martha M. Larson

John H. Rossmeisl

Nick Dervisis

Jeryl C. Jones

June 16, 2016

Blacksburg, VA

Keywords: Diffusion weighted MRI, Canine regional lymph node metastases

Diffusion Weighted Magnetic Resonance Imaging in the Differentiation between Benign and Metastatic Lymph Nodes in Canine Patients with Head and Neck Disease

Jessica Anne Stahle

Abstract

In dogs with large primary tumors, regional lymph node involvement or evidence of distant metastasis can have worse prognoses and significantly decreased survival. Lymph node size alone has been shown to be insufficient as a predictor for the accurate clinical staging of some canine neoplasia, including oral malignant melanoma. However, regional lymph nodes of the oral cavity, such as the medial retropharyngeal lymph nodes, are difficult to access for routine sampling. Diffusion weighted magnetic resonance imaging (DWI) has demonstrated the ability to differentiate metastatic from inflammatory/benign lymph nodes in clinical studies with human cancer patients through the calculation of quantitative values of diffusion termed apparent diffusion coefficients (ADC). The objective of this exploratory study was to evaluate DWI and ADC as potential future methods for detecting malignant lymph nodes in dogs with naturally occurring disease. We hypothesized that DWI would identify significantly different ADC values between benign and metastatic lymph nodes in a group of canine patients with head or neck disease.

Our results demonstrated that two of four observers identified a significant difference between the mean ADC values of the benign and metastatic lymph nodes. When data from all four observers were pooled, the difference between the mean ADC values of the benign and metastatic lymph nodes approached but did not reach significance (P-value: 0.0566). Therefore, our hypothesis was not supported. However, DWI does show promise in its ability to differentiate benign from metastatic lymph nodes, and further studies with increased patient numbers are warranted.

Diffusion Weighted Magnetic Resonance Imaging in the Differentiation between Benign and
Metastatic Lymph Nodes in Canine Patients with Head and Neck Disease

Jessica Anne Stahle

General Audience Abstract

In dogs with cancer, knowledge of the spread of disease to lymph nodes and other parts
of the body can be useful in establishing prognosis and deciding on the best therapeutic course.
To determine if lymph nodes have been infiltrated with cancer, lymph nodes are sampled to
obtain cellular or tissue samples which can be microscopically evaluated. However, some lymph
nodes are difficult to access, therefore, a non-invasive method of evaluation could be a useful
tool in staging canine cancer. In human clinical studies, a specific type of magnetic resonance
imaging termed diffusion weighted imaging (DWI) has demonstrated the ability to differentiate
between lymph nodes that are infiltrated with cancer (metastatic) from those that are not
(benign). Diffusion weighted imaging is able to differentiate between these two types of lymph
nodes through establishing a numeric value called an apparent diffusion coefficient (ADC) value
for each lymph node. Our study aimed to evaluate the ability of DWI to differentiate between
metastatic and benign lymph nodes in a group of canine patients with head or neck disease.

Our results demonstrated that two of four observers identified a significant difference
between the mean ADC values of the benign and metastatic lymph nodes. When data from all
four observers were pooled, the difference between the mean ADC values of the benign and
metastatic lymph nodes approached but did not reach significance. Therefore, our hypothesis
was not supported. However, DWI does show promise in its ability to differentiate benign from
metastatic lymph nodes, and further studies with increased patient numbers are warranted.

Table of Contents

List of Equations

List of Tables

List of Figures

CHAPTER 1: LITERATURE REVIEW

A. Lymphatic system

As blood flows through the arterial capillary bed, some fluid (as well as nutrients, electrolytes, and small proteins) escapes into surrounding tissue spaces. The majority of this fluid is reabsorbed into the venous capillaries, with the remaining fluid entering the lymphatic capillaries as lymph. Lymph nodes are located along the course of lymph vessels, with the lymph vessels entering the lymph nodes termed afferent vessels, and those exiting the lymph nodes termed efferent vessels (Benzuidenhout 2013). Lymph nodes receive afferent lymphatic vessels from specific regions of the body (Fry 2012).

Lymph nodes function to filter lymph, expose antigens to circulating lymphocytes, and to act as germinal centers for lymphocytes (Cowell 2008). Lymph nodes each consist of an outer capsule that contains muscle fibers, while internally, a poorly defined cortex and medulla are present (Benzuidenhout 2013). Multiple afferent lymphatic vessels enter through the outer capsule, with the lymph then passing into the subcapsular sinus. Fibrous trabeculae and fibroblastic reticular cells support the lymph node, and act to guide interaction of lymphocytes and antigen presenting cells. Multiple lymphoid follicles are noted within the outer cortex, with these follicles surrounded by lymph filled sinuses. There are two types of lymphoid follicles, primary and secondary. The primary lymphoid follicles contain mostly resting B lymphocytes and dendritic cells. B lymphocytes that recognize antigen are activated and proliferate to form secondary lymphoid follicles, which are characterized by germinal centers. These germinal centers are regions that support proliferation and development of B lymphocytes. The inner cortex of the lymph node contains T lymphocytes and high endothelial venules (Fry 2012).

The medulla of the lymph node is made up of medullary cords and medullary sinuses. The medullary cords contain macrophages and lymphocytes, and are surrounded by the medullary sinuses which are lined by fibroelastic reticular cells (Fry 2012). The macrophages within the medullary cords phagocytose material within the incoming lymph. The efferent lymph vessels carry lymph out of the lymph nodes to enter major efferent ducts, with eventual return of the lymph into the blood. Prior to returning to the blood, the lymph may pass through one or more additional lymph nodes downstream (Haig, Hopkins et al. 1999).

B. Lymph centers of the canine head

Lymphocenter is a term used to denote a lymph node or group of lymph nodes that occur consistently in the same location and receive lymphatic vessels from the same region (Fry 2012). There are three lymphocenters in the canine head: 1.) parotideum 2.) mandibulare and 3.) retropharyngeum (Benzuidenhout 2013). The parotid lymph nodes make up the lymphocentrum parotideum, located at the rostral base of the ear. These lymph nodes drain lymph from several cephalic muscles (e.g. temporal, masseter, zygomatic), the lacrimal apparatus, and several bones of the skull. The mandibular and buccal lymph nodes create the lymphocentrum mandibulare. The mandibular lymph nodes usually consist of a group of two or three lymph nodes positioned ventral to the angle of the mandible, in the region of the linguofacial vein. The mandibular lymph nodes drain lymph from portions of the head not drained by the parotid lymph nodes, including the palatal region, tongue, and pharynx (Benzuidenhout 2013). The buccal lymph nodes are located in the region of the confluence of the facial and superior labial veins. They may be unilateral, bilateral, or absent, and are reportedly only present in a minority of dogs (Casteleyn, van der Steen et al. 2008). A medial and occasionally a lateral retropharyngeal lymph node make up the canine lymphocentrum retropharyngeum. The medial retropharyngeal

2

lymph node is the largest lymph node of the head. The afferent lymph vessels of the medial

retropharyngeal lymph nodes come from structures such as the tongue, pharyngeal area, larynx,

salivary glands, esophagus, and non-cutaneous, non-mucous structures of the neck.   The medial

retropharyngeal lymph nodes also receive efferent lymph vessels from the parotid, mandibular,

and lateral retropharyngeal lymph nodes (Benzuidenhout 2013).

C. Lymphadenopathy

Lymphadenopathy (which can lead to lymphadenomegaly) can occur secondary to

malignant disease such as neoplasia (metastatic or infiltrative disease) or benign disease

including: hyperplasia (reactive lymphadenopathy), lymphadenitis, immune stimulation, or

extramedullary hematopoiesis (Cowell, Dorsey et al. 2003).   The presence of metastatic or

infiltrative disease within a lymph node is important in disease staging, and has been found to be

valuable in establishing prognosis in dogs (Hillers, Dernell et al. 2005). It has been suggested

that lymph node size alone is insufficient for accurate clinical staging of certain canine neoplastic

diseases (Williams and Packer 2003). Additionally, it has been shown that statistically

significant relationships exist between body weight, age and lymph node size in dogs (including

medial retropharyngeal lymph nodes) (Burns, Scrivani et al. 2008). Therefore, cytologic or

histologic examination of regional lymph nodes is recommended for more accurate staging

(Williams and Packer 2003).

Cytologic examination provides a rapid, minimally invasive, inexpensive method of

lymph node evaluation. Small mature lymphocytes are the most prominent cells within normal

lymph nodes, accounting for 75-85% of all nucleated cells (Cowell 2008). Reactive/hyperplastic

lymph nodes demonstrate lymphoid proliferation in response to antigenic stimulation (Cowell,

Dorsey et al. 2003). Lymph node enlargement due to hyperplasia is caused by expansion of the

cortex by increased numbers of lymphoid follicles, which usually contain active germinal centers (Fry 2012). Lymphadenitis is characterized by an accumulation of inflammatory cells, with inflammation considered likely if the cell population is >5% neutrophils or >3% eosinophils without significant blood contamination (Cowell 2008). Single neoplastic cells or clusters of cells that become deposited within a lymphoid sinus via travel through an afferent lymphatic vessel may cause metastatic disease within a lymph node. The neoplastic cells may proliferate within the lymph node, and malignant cells can be sent via efferent lymphatics to the next lymph node along the lymphatic chain (Fry 2012). Metastatic neoplasia within a lymph node is recognized by the presence of either an abnormally high number of cells that are usually present in low numbers (e.g. mast cells) or by the presence of cells that are not normally found within a lymph node and demonstrate malignant criteria such as anisokaryosis and high nucleus to cytoplasm ratio (Cowell, Dorsey et al. 2003).

Reported limitations of cytology include poor ability to evaluate architecture of sampled tissue, and difficulty in acquiring a diagnostic sample in tissues with poor exfoliation (Vos, van den Ingh et al. 1989). Histopathologic diagnosis is often considered the gold standard against which cytologic evaluation is compared. One study reports the sensitivity of cytologic examination in veterinary patients ranges from 33.3 to 66.1% (Cohen, Bohling et al. 2003). A 2001 study (Langenbach, McManus et al. 2001) evaluated the sensitivity and specificity of physical examination, fine-needle aspiration, and needle core biopsy sampling of regional lymph nodes in a group of dogs and cats with solid tumors. The conclusions of this study included that physical examination alone (i.e. palpation) was not a reliable method for determining metastatic lymph node disease, fine-needle aspiration is a reliable method of assessing regional lymph nodes (cytologic sensitivity: 100%, specificity: 96%), and needle core biopsy is a reasonably

accurate method of assessing lymph nodes (needle core biopsy sensitivity: 64%, specificity: 96%). This study therefore found needle core biopsy to be less sensitive than fine needle aspiration, possibly due to staining differences and the small size of the specimen obtained with needle core biopsy.

D. Sonography of lymph nodes (veterinary medicine)

Ultrasonographic assessment of lymph nodes is performed regularly in dogs. Normal echogenicity of lymph nodes is reported as uniform, isoechoic, or slightly hypoechoic to surrounding tissues with abnormal lymph nodes reported as non-uniform and either hypoechoic or anechoic. Normal lymph nodes are longer in length than thickness, with a short- to long-axis ratio providing a quantitative assessment of size and shape. Irregular margination of lymph nodes may be interpreted as a sign of malignancy (Nyman and O'Brien 2007). Doppler ultrasonography can be used to evaluate the vascular structures of lymph nodes. The lymph node hilus is the normal site of entry and exit for nodal blood. Normal lymph nodes demonstrate mostly hilar vascularity or appear avascular, whereas reactive lymph nodes demonstrate prominent hilar vascularity due to enlargement of vascular diameter and an increase in blood flow. Metastatic lymph nodes often demonstrate a peripheral pattern of perfusion, thought to be due to deposition of tumor cells within the sinuses of the lymph node, with tumor angiogenesis leading to aberrant vessel formation. (Nyman and O'Brien 2007).

A 2005 study (Nyman, Kristensen et al. 2005) evaluated 318 superficial lymph nodes in canines to evaluate the ability of ultrasonography to differentiate between normal and abnormal lymph nodes. The short- to long-axis ratio (S/L) was significantly different between normal and malignant (both metastatic and lymphoma) lymph nodes, with lymphoma nodes demonstrating a S/L > 0.7, and benign lymph nodes having an S/L < 0.6 Benign lymph nodes demonstrated a

primarily hilar flow, while metastatic lymph nodes showed peripheral flow. Two-thirds of the lymphoma group lymph nodes demonstrated mixed hilar and peripheral flow, while the other third had hilar flow. Pulsatility indices (PI) defined as: ((peak systolic velocity – end diastolic velocity)/time averaged maximum velocity) and resistive indices (RI) defined as: ((peak systolic velocity – end diastolic velocity)/peak systolic velocity) were calculated. A significant difference was found between the PI values of benign lymph nodes (mean PI: 1.07) versus those of the malignant lymph nodes (lymphoma PI: 1.27, metastatic PI: 1.72). It is thought that increased vascular resistance in the vessels of lymph nodes containing metastatic disease is due to compression of the vessels by tumor cells (Choi, Lee et al. 1995). A discriminant analysis showed that the use of the three aforementioned parameters (size of the lymph node, distribution of vascular flow within the lymph node, and PI) could most accurately classify the canine lymph nodes into benign or malignant groups (Nyman, Kristensen et al. 2005).

A second 2005 study (Salwei, O'Brien et al. 2005) sought to evaluate the ability of contrast (lipoprotein-encapsulated inert gas) harmonic ultrasound to provide improved conspicuity of lymph node angioarchitecture when compared to power Doppler. The study consisted of eleven dogs with multicentric malignant melanoma. The authors reported that identification of features of malignant angioarchitecture was improved with the use of contrast tissue harmonic ultrasound, with malignant features including displacement of the central hilar vessels, presence of aberrant vessels, and presence of subcapsular and pericapsular vessels (Salwei, O'Brien et al. 2005).

The association between sonographic heterogeneity and malignancy within feline and canine abdominal lymph nodes was evaluated in 2007 (Kinns and Mai 2007). Within the studied group of canine lymph nodes, twenty-one heterogeneous lymph nodes were identified as

6

malignant, with only two identified as benign. Within the studied group of feline lymph nodes, seven heterogeneous lymph nodes were identified as malignant, as well as eleven benign.   The conclusions drawn from this study were that canine abdominal lymph node heterogeneity is more commonly associated with malignant lymphadenopathy, and that feline abdominal lymph node heterogeneity is non-specific (Kinns and Mai 2007)

A 2011 study (De Swarte, Alexander et al. 2011) compared the sonographic features of benign and neoplastic deep canine lymph nodes. Authors reported that the maximum short- to long-axis ratio was significantly increased in the neoplastic group. The vast majority of the lymph nodes in this study were hypoechoic, regardless of group, with the authors stating that echogenicity is not a useful indicator of lymph node malignancy. In this study, Doppler evaluation was only possible in 77% of the lymph nodes, with no statistically significant difference found for any Doppler criteria.   The study also sought to evaluate combining songraphic features of lymph nodes, as such combination has been reported to aid in differentiation of canine benign and neoplastic lymph nodes (Nyman, Kristensen et al. 2005). However, the only statistically significant difference between benign and neoplastic lymph nodes was for the combination of contour regularity and appearance of perinodal fat, with 50% of benign lymph nodes demonstrating regular contour with normal perinodal fat versus only 10% of neoplastic nodes. In the discussion of this study, the authors point out there is a lack of complete reliability of sonographic features of benign vs. malignant lymph nodes, and also mention that sampling of deep or small lymph nodes may be hazardous (De Swarte, Alexander et al. 2011).

E. Cross sectional imaging of lymph nodes

Lymph nodes can be imaged and evaluated using cross sectional imaging such as magnetic resonance imaging (MRI) and computed tomography (CT).   The MR appearance of

presumed normal lymph nodes of the canine head and neck has been described as homogeneous, isointense signal in T1-weighted images and hyperintense on T2-weighted images when compared to muscle (Kneissl and Probst 2006). Additionally in this study, the size of the canine medial retropharyngeal lymph node (MRPLN) was found to be approximately 30-70mm x 10mm x 5-10mm (length x height x width), with the length of the mandibular lymph nodes found to vary from 10 to 25mm (Kneissl and Probst 2006). A study evaluating the MR appearance of neoplastic versus inflammatory medial retropharyngeal mass lesions in both dogs and cats found that the presence of perinodal contrast enhancement and muscle contrast enhancement was significantly more likely to be associated with an inflammatory rather than neoplastic etiology (Johnson, Elders et al. 2015). A 2012 study (Pokorny, Hecht et al. 2012) evaluating the MRI appearance of canine mast cell tumors found that all imaged lymph nodes (including axillary, parotid, mandibular, popliteal, medial iliac, medial retropharyngeal and superficial cervical) when compared to muscle were isointense on T1-weighted images, hyperintense on T2-weighted and STIR (fat suppressed) images, and were moderately to strongly contrast enhancing. This study found that metastatic lymph nodes were significantly larger than the contralateral lymph nodes. They also reported that although lymph node heterogeneity on T2-weighted and post contrast T1-weighted images was more common in metastatic lymph nodes (vs. normal lymph nodes), this finding was not significant (Pokorny, Hecht et al. 2012).

The CT characteristics of normal canine cephalic lymph nodes have also been described. Kneissl and Probst (2007) found that mandibular and medial retropharyngeal lymph nodes could be consistently identified on CT, and when compared to muscle, normal lymph nodes were slightly hypodense and demonstrated homogeneous parenchyma as well as homogeneous contrast enhancement. A hypodense, triangular region that was presumed to be the hilus was

8

noted to indent some of the lymph nodes.   The size of the MRPLN was found to be 30-70mm x 10mm x 5-10mm (length x height x width). The parotid lymph node was not consistently visualized in this study (Kneissl and Probst 2007).   Computed tomographic characteristics of canine tracheobronchial lymph node metastasis have been described (Ballegeer, Adams et al. 2010). This study found a significant association between the presence of rim and/or heterogeneous contrast enhancement and lymph node metastasis, though this type of enhancement pattern was also noted in patients with severe granulomatous lymphadenitis and lymphoid hyperplasia (Ballegeer, Adams et al. 2010).   A more recent study evaluated the CT characteristics of MRPLN in cats with rhinitis and nasal neoplasia (Nemanic, Hollars et al. 2015). This study found that an abnormal hilus, height asymmetry, and decreased precontrast heterogeneity (i.e. homogeneous parenchyma) were significantly associated with nasal neoplasia. This study also found that the appearance of the MRPLN was significantly different between cats with lymphoma and carcinoma, with the MRPLN of cats with lymphoma demonstrating more contras enhancement and were found to be more homogeneous than those with carcinoma (Nemanic, Hollars et al. 2015)

Morphologic imaging techniques such as CT provide identification of enlarged lymph nodes, although reportedly in humans, accurate differentiation of benign from malignant lymph nodes cannot be made (Abdel Razek, Soliman et al. 2006).   A study regarding the evaluation of human cervical lymph nodes in patients with head and neck cancer (Hoang, Vanka et al. 2013) points out that size alone is not a reliable marker of malignancy. The presence of nodal necrosis is considered a characteristic of metastatic lymph nodes, with human studies describing the MRI appearance of lymph node necrosis as areas of low signal intensity on T1-weighted images that correspond to high signal intensity on T2-weighted images and demonstrate rim enhancement on

post contrast sequences (Chong, Fan et al. 1996). Although nodal necrosis is a considered a valuable sign of metastatic involvement, partial volume artifact of the normal fatty hilus can mimic nodal necrosis (Hoang, Vanka et al. 2013) and care must be taken in evaluating this finding singularly.

Human studies on the use of metabolic imaging concluded that photon emission tomography (PET) can aid in the differentiation of benign and malignant lymph nodes (Szakall, Esik et al. 2002). When compared with CT, MRI, or sonography, 18F-fluorodeoxyglucose (FDG) PET increased sensitivity for nodal metastases from 79% to 85% and increased specificity from 80% to 86% (Kyzas, Evangelou et al. 2008). FDG-PET has been determined to be a useful tool for detection of lymph node involvement in both canine lymphoma and cutaneous mast cell tumor (LeBlanc, Jakoby et al. 2009). However, PET imaging utilizes ionizing radiation and is not readily accessible to most veterinary patients.

F. Physics of diffusion weighted magnetic resonance imaging

The image contrast in diffusion weighted magnetic resonance imaging is created by the random microscopic motion of water molecules (Bammer 2003). Molecular diffusion is also known as Brownian motion, and refers to the idea that any type of molecule in fluid is randomly displaced due to collision with other molecules and thermal molecular motion. This random motion can be described by a displacement distribution, which demonstrates the proportion of molecules undergoing displacement in a specific direction to a specific distance (Hagmann, Jonasson et al. 2006). Brownian motion represents uninhibited or free diffusion, which is in contrast to the movement of water molecules within biologic tissues. Biologic tissues consist of heterogeneous materials that contain compartments and barriers (such as cell membranes), that create different diffusivities and varying degrees of restricted diffusion (Koh and Collins 2007).

The degree of restriction to water diffusion within biologic tissue is proportional to the overall tissue cellularity and the integrity of the cell membranes. Highly cellular tissues with intact cell membranes (as can be seen in tumor tissue) demonstrate restricted diffusion, as water motion is restricted within both the intra- and extracellular spaces. Tissues with low cellularity or decreased cell membrane integrity (as can seen in cystic or necrotic tissues) create a larger extracellular space for water motion or can allow for water motion between the extra- and intracellular compartments (Koh and Collins 2007).

Diffusion weighted images (DWI) are created by the application of two equal (i.e. symmetric) gradient pulses, most commonly to a spin echo (SE) sequence. In a basic SE sequence, a 90-degree pulse is initially applied, flipping the net magnetization vector into the transverse plane. A 180-degree pulse is then applied at a time equal to one-half of echo time (TE) to re-phase the spinning nuclei. At total TE, an echo (signal) is produced and read (Bitar, Leung et al. 2006).   To create a diffusion weighted image, the first gradient pulse is applied, creating a phase shift at time = 0. The 180-degree pulse is then applied to reverse the phase shift created by the first gradient pulse. The second gradient pulse is then applied. Molecules that remain in the same position during the applications of the two gradient pulses will experience de-phasing followed by re-phasing, and MR signal intensity will be maintained. Molecules that have moved during the application of the gradients will experience a phase shift that will result in reduction of the intensity of the MR signal. The greater the distance a molecule moves between the applications of the gradient pulses, the higher the phase shift, and the greater the reduction in MR signal. Therefore, the reduction in signal intensity is proportional to the degree of molecule motion (Bitar, Leung et al. 2006, Hagmann, Jonasson et al. 2006).   Diffusion weighted images are also usually acquired using echo-planar imaging (EPI), in which a single echo train is used to

collect data from all lines of k-space during one repetition time (TR) (Bitar, Leung et al. 2006). Echo planar imaging sequences allow image acquisition within a fraction of a second, although EPI sequences are very susceptible to main field inhomogeneity and chemical shift, which can lead to image degradation (Bammer 2003).

Factors affecting the sensitivity of the DWI to water motion include gradient amplitude, duration of the applied gradients, and the time interval between the application of the gradients. These three factors are proportionally affected by a factor known as the b-value. A b-value is an extrinsic contrast parameter that controls how much the apparent diffusion coefficient (ADC) value of a specific tissue contributes towards image weighting (Westbrook 2011). B-values have units of seconds per square millimeter (s/mm^2) and are a representation of the overall motion sensitivity of the sequence, calculated by the equation: $b = \gamma^2 \ G_i^2 \ \delta^2 (\Delta - \delta/3)$ (**Equation 1**) (Neil 1997). Therefore, changing the b-value can vary the diffusion sensitivity of a DWI sequence. Generally the larger the b-value, the greater the degree of signal attenuation from moving water molecules. When small b-values (e.g. 50 to 100 s/mm^2) are used, MR signal attenuation may be seen with water molecules that demonstrate large degrees of motion, whereas larger b-values (e.g. 1000 s/mm^2) may be needed to perceive slow-moving water molecules or small diffusion distances (Koh and Collins 2007). Usually DWI sequences are obtained using at least two different b-values.

Acquisition of DW images using at least two b-values makes a quantitative analysis of diffusion possible through the creation of an apparent diffusion coefficient (ADC) map image. The ADC represents the net displacement of molecules diffusing across an area of tissue per second (Westbrook 2011). Apparent diffusion coefficient map images are termed ADC rather than just diffusion coefficient because within biologic systems, the motion of water molecules is

unlikely to be due to only diffusion. Instead, such water motion is likely due to a combination of Brownian motion and movement of molecules across cell membranes (Neil 1997). Each pixel in an ADC map image is calculated according to the equation: $ADC = (1/\ b_1 - b_0)\ \ln(S[b_0]/S[b_1])$ (**Equation 2**) (Kwee, Takahara et al. 2008). Therefore, an ADC map image is acquired via post-processing, and acts as a true representation of diffusion in a tissue, such that areas of restricted diffusion will demonstrate low signal and regions of free diffusion will demonstrate high signal. It is important to note that this is opposite to the signal that will be observed on DWI, where regions of restricted diffusion will demonstrate high signal, and regions of free diffusion will demonstrate low signal (Koh and Collins 2007).

Regions of interest (ROIs) can be drawn on the ADC images, in order to determine quantitative values of diffusion for certain tissues. When such ROIs are drawn, the resultant ADC values are expressed in units of mm^2/s. In addition to allowing for the determination of quantitative values of diffusion, ADC map images can be used to identify the presence of a phenomenon called T2-shinethrough. On DWI, signal intensity depends not only on water diffusion but also on the T2 relaxation time. Therefore, an area with a long T2 relaxation time may demonstrate high signal on a DWI, possibly mistaken for a region of true restricted diffusion. The ADC map is independent of magnetic field strength, and can overcome the effects of T2-shinethrough (Koh and Collins 2007). Therefore, regions of T2-shinethrough will demonstrate high signal on both DWI and ADC map images. Additionally, two other phenomenon can occur on DWI: T2 washout and T2 blackout. T2 washout represents a region of isointensity on a DW image, and is due to a balance between inherent T2-weighted hyperintensity and an increased ADC value (free diffusion), often seen associated with vasogenic edema (Hiwatashi, Kinoshita et al. 2003). T2 blackout represents a region of hypointensity on

13

DWI that is due to inherent T2-weighted hypointensity, often seen associated with hematomas and predominantly due to susceptibility effects (Hiwatashi, Kinoshita et al. 2003).

As noted above, ADC values are termed apparent diffusion coefficient rather than just diffusion coefficient because within biologic systems, the motion of water molecules is unlikely to be due to only diffusion.   It has been proposed that two types of diffusion occur within tissues. The first type of diffusion is represented by a coefficient "D" which represents the molecular motion of water within tissues. The second type of diffusion, termed pseudodiffusion, is represented by a coefficient "D*" and is associated with capillary blood flow (Le Bihan 2008). A method of MR imaging termed intravoxel incoherent motion (IVIM) imaging is able to distinguish between pure molecular diffusion and blood perfusion (microcirculation) (Luciani, Vignaud et al. 2008). Signal intensity in IVIM can be calculated using the equation: $S_b / S_0 =$ (1-f) exp(-bD) + (f) exp(-bD*) (**Equation 3**) (Le Bihan, Turner et al. 1989).

G. Early applications of diffusion weighted imaging (human medicine)

Diffusion weighted imaging was first introduced in 1965 (Stejskal 1965), although *in vivo* studies regarding diffusion weighted imaging did not begin until the late 1980s (Le Bihan, Breton et al. 1986) (Merboldt, Bruhn et al. 1989). One study concluded that such *in vivo* studies were compromised by contributions from motion such as microcirculation (e.g. perfusion) and macroscopic motion (breathing motion, patient movement) (Merboldt, Bruhn et al. 1989). With the development and availability of echo planar imaging (EPI) for use in clinical MR scanners, the effect of motion artifact on diffusion weighted images was decreased, since the entire set of echoes could be acquired in a short period (Turner, Le Bihan et al. 1990).

The utility of diffusion weighted imaging for the early detection of cerebral ischemic insults was demonstrated in the early '90s (Moseley, Cohen et al. 1990). In this study, a single

middle cerebral artery and both common carotid arteries were occluded prior to imaging. Through region of interest (ROI) analyses, apparent diffusion coefficient (ADC) values were measured and found to be nearly three times lower within the ischemic regions when compared to apparently normal tissue. The authors proposed that hyperintensity observed on the DWI sequences, which corresponded to the regions of lower ADC values (regions of restricted diffusion), may represent intracellular swelling due to cytotoxic edema, with water molecules originally positioned within the extracellular space located within the intracellular compartment. This study also demonstrated that these regions of hyperintensity seen on the DWI sequences were visible as early as 45 minutes after the onset of ischemia (Moseley, Cohen et al. 1990). The theory that decreased ADC values in regions of ischemia are due to a shift of extracellular to intracellular water was further supported by other studies. One such study proposed that after the onset of ischemia, tissue ATP reserves are depleted, leading to failure of the $Na^+ K^+$ ATPase pump. This in turn causes water and ions to pass from the extracellular space into the intracellular space, resulting in a decreased ADC value (Benveniste, Hedlund et al. 1992).   With time, cells in ischemic regions lyse and macrophage activity increases along with the development of vasogenic edema, which is more readily imaged on conventional T2-weighted images. Additionally with time, regions of ischemia will demonstrate the opposite appearance of an acute ischemic region, appearing hyperintense on ADC and hypointense on DWI (Roberts and A. 2003).

The addition of diffusion weighted MR imaging to conventional MR sequences has been demonstrated to improve the accuracy of identifying acute ischemic brain lesions. One study reported that when utilizing DWI, at least one acute lesion was identified in 94% of a group of patients with a final diagnosis of stroke, compared to lesions identified in approximately 71-80%

of the patients when only conventional MR sequences (T2-weighted, PD-weighted, or FLAIR) were used (Lansberg, Norbash et al. 2000). A recent study assessed the diagnostic accuracy of a brain MR protocol consisting of a limited number of sequences was performed. This study found that a four- sequence brain MRI protocol (including sagittal T1-weighted, axial T2-weighted FLAIR, axial DWI, and axial T2*-weighted images) reliably detects nearly all non-contrast enhancing brain findings in patients without a known history of neurologic disease undergoing evaluation for a new neurologic problem (Mehan, Gonzalez et al. 2014)

An additional type of diffusion imaging termed diffusion tensor imaging (DTI) was developed in the mid 1990s (Basser, Mattiello et al. 1994). In DTI, certain tissues such as brain white matter and skeletal muscle demonstrate anisotropic diffusion, meaning that observed echo intensity is dependent upon the tissue's orientation with respect to the applied MR gradient (Basser, Mattiello et al. 1994). Anisotropy is a quantitative parameter that can be representative of the degree to which diffusion varies in different directions (Shimony, McKinstry et al. 1999). Anisotropy MR images can depict white matter features that may not be seen on conventional MR sequences, allowing for identification in subtle white matter anatomic differences. There is some degree of consistency regarding anisotropy values and mean principal diffusion coefficients across subjects, and statistically significant differences have been noted between anisotropy values in different regions of the brain (Shimony, McKinstry et al. 1999). The use of diffusion tensor imaging continues to be studied to evaluate and characterize various diseases processes as well as describe normal neuronal structures (Hannoun, Durand-Dubief et al. 2012) (Walker, Chang et al. 2016).

H. Diffusion weighted imaging outside of the central nervous system (human medicine)

In the late 1990s, diffusion-weighted MR imaging was used to characterize abdominal organs and hepatic lesions (Muller, Prasad et al. 1994) (Namimoto, Yamashita et al. 1997). Advancements including parallel imaging techniques (such as sensitivity encoding (SENSE)), along with aforementioned echo planar imaging (EPI) allowed for improved acquisition of diffusion-weighted images (DWI) of the body.   SENSE enables k-space to be filled more efficiently by filling multiple lines of k-space per TR through the coupling of coils to allow them to acquire data simultaneously, with lines of k-space assigned to certain coils (Westbrook 2011).

In their 2004 study, Takahara, Yutaka et al. described a technique termed diffusion weighted whole body imaging with background body signal suppression (DWIBS). Prior to this point, whole body DWI (including malignancy screening) was limited by insufficient fat suppression and thick slice acquisition. In order to generate a three-dimensional (3D) display (as that easily created with PET scans), thin slices are necessary, however a breath-hold technique (designed to limit physiological motion) limited the use of thinner slices. This group demonstrated that free breathing scanning worked well, allowing for longer scan times and therefore more slices with multiple signal averaging and resultant higher signal to noise ratio (Takahara, Yutaka et al. 2004).   Diffusion weighted imaging using free breathing can be performed because the two gradients are applied within a very small time interval, and respiratory motion can be considered coherent motion. The applied gradients only create signal attenuation in the case of incoherent motion (e.g. diffusion), so the MR signal is not affected by the coherent respiratory motion (Kwee, Takahara et al. 2008). The 2004 Takahara study also demonstrated that thin slice STIR-EPI (short T1 inversion recovery) is feasible, produces excellent fat suppression, and results in the ability to produce 3D body DW images (Takahara,

Yutaka et al. 2004).   Utilizing this STIR-EPI combination sequence, some tissues are suppressed

(e.g. vessels, muscle, fat, most organs), some normal tissues are visualized (e.g. prostate, testes,

ovaries, spleen, tonsils, lymph nodes), and some abnormal tissues are also visualized (tumors,

abscesses) (Takahara 2005). When compared to other cross sectional imaging methods (i.e.

PET, CT), DWIBS does not involve ionizing radiation and does not require contrast

administration (Takahara 2005).

In addition to DWIBS sequences, DWI currently can be applied to the human body

utilizing breath hold imaging or non-breath hold imaging (Koh and Collins 2007). Breath hold

imaging can be used when a target region (e.g. organ) is to be assessed. This type of DWI often

utilizes SE EPI combined with parallel imaging (e.g. SENSE) and some type of fat suppression

(e.g. SPAIR). Disadvantages of the breath hold technique reportedly include a limited number of

b-value images that can be obtained in a short period (breath hold), decreased signal to noise

ratio, and greater sensitivity to pulsatile and susceptibility artifacts (Koh and Collins 2007).

Non-breath hold SE EPI also typically uses some type of fat suppression (e.g. SPAIR, STIR).

Non-breath hold imaging allows for longer acquisition times, and therefore makes the use of

multiple b-values or high b-values possible (Koh and Collins 2007).

I. Applications of non-CNS diffusion weighted imaging, excluding lymph nodes (human

medicine)

Since its development, an important extra-cranial use of DWI has been oncologic, with

one such application regarding tumor characterization. Diffusion weighted imaging provides a

way to assess the entire tumor, as compared to tissue sampling which is not only invasive but

may not be representative of the entire tumor (Lang, Wendland et al. 1998). An early 2001 study

attempted to determine if ADC values could be used to characterize head and neck lesions

(Wang, Takashima et al. 2001). This research group found that the mean ADC values of benign cystic and benign solid lesions were significantly higher than those of malignant tumors. It was suggested that these differences in ADC values may reflect the differences in histopathologic features of the benign versus malignant lesions (Wang, Takashima et al. 2001)

A 2002 study (Guo, You-Quan et al. 2002) evaluated the ability of DWI to distinguish benign from malignant breast lesions through the comparison of the mean ADC values for each group (benign and malignant).   Similar to the above-mentioned 2001 study, this study found a significant difference between the mean ADC values of these groups, with the ADC values of the malignant lesions lower than those of the benign lesions. The study also demonstrated that the ADC values of the breast tumors correlated well with tumor cellularity, with malignant tumors having a higher cellularity and lower ADC values than benign lesions (Guo, You-Quan et al. 2002).

Other studies have found similar results as those noted above, with reduced ADC values reported for malignant tumors (Issa 2002) (Srinivasan, Dvorak et al. 2008) (Abdel Razek, Gaballa et al. 2009) (Wan, Lee et al. 2016). However, when ADC values are used to differentiate between benign and metastatic lesions, it is important to note that necrotic regions that may be contained within benign or malignant lesions can affect the ADC value. This concept was demonstrated in a 2000 study (Lyng, Haraldseth et al. 2000) which sought to determine whether ADC values could be used as a measure of cell density and necrotic fraction of tumors.   This study identified a significant correlation between the ADC values of viable tumor tissue and cell density, with ADC values decreasing as cell density increased (Lyng, Haraldseth et al. 2000).   It has been proposed that highly cellular tissues have a large fraction of intracellular water, and that lower ADC values may be seen associated with intracellular water

19

due to increased barriers to diffusion within the intracellular compartment (Szafer, Zhong et al. 1995, Lyng, Haraldseth et al. 2000). Also, highly cellular tissues have a small extracellular compartment, so there is lower mobility of extracellular water and resultant lower ADC values (Lyng, Haraldseth et al. 2000). In one study (Lyng, Haraldseth et al. 2000), mice with tumors due to several amelanotic human melanoma xenograft lines including D-12 and U-25 were evaluated. Necrotic portions of tumors were significantly correlated with increasing ADC values within the D-12 line, thought to represent increased water motion within areas of necrosis. However, the U-25 tumors did not demonstrate an increase in ADC value with increasing necrotic fraction. It was proposed that this difference in ADC value associated with necrosis may be due to the characteristics of the tumor. D-12 tumors reportedly demonstrated a single region of necrosis, while the U-25 tumors demonstrated several small regions of necrosis throughout the tumor. The authors proposed that the distribution of necrotic regions within the U-25 tumors could therefore create a high necrotic fraction, but with small areas of necrosis versus the single larger necrotic region noted within the D-12 line (Lyng, Haraldseth et al. 2000). This difference in the distribution of necrotic regions could lead to partial volume effects, in that viable tissue could contribute to the ADC value of most pixels, including regions identified histologically as necrotic. Therefore, the use of ADC values in evaluating cell density and necrotic fraction in tumors that demonstrate several small areas of necrosis (versus a single region of necrosis) was determined to be potentially problematic (Lyng, Haraldseth et al. 2000).

In addition to tumor characterization, another non-CNS application of DWI includes monitoring tumor response to treatment. Possible cellular changes resulting from anti-cancer therapy include cell membrane defects and enlarged extracellular space with a resultant increase in water diffusion and therefore variation in the ADC value of the tumor (Moffat, Chenevert et

al. 2005). However, initially post therapy, a transient decrease in the ADC value of a tumor may be observed, thought to represent cell swelling (Moffat, Chenevert et al. 2005) (Thoeny, De Keyzer et al. 2005). Subsequent cellular necrosis and lysis, as well as apoptosis can then lead to increases in ADC values (Moffat, Chenevert et al. 2005). DWI has also been utilized to predict response to therapy. In a recent study that evaluated patients with rectal cancer, it was found that ADC values prior to treatment (neoadjuvant chemoradiotherapy) were significantly lower in the patients that demonstrated a better (greater pathological) response to therapy (Doi, Beppu et al. 2015). It has been suggested that necrotic areas, which would lead to higher pre-treatment ADC values, may be less sensitive to chemoradiotherapy (Doi, Beppu et al. 2015). However, studies with findings contradictory to those above have been recorded. Such contradictory studies include a 2011 study, which found no significant differences in the pre-treatment ADC values in tumors that responded to therapy versus those that did not respond, in a group of patients with rectal cancers (Kim, Lim et al. 2011). This group therefore concluded that mean ADC values may be limited in predicting outcome of treatment with chemoradiotherapy.

A final non-CNS application of DWI has been in the area of functional evaluation. A 1999 study evaluated the relationship between ADC values of the kidney and renal disease (Namimoto, Yamashita et al. 1999). This study found that the ADC values of both the renal cortices and medullary regions in patients with chronic renal failure and acute renal failure were significantly lower than those of normal kidneys. It was proposed that fibrosis associated with chronic renal failure leads to decreased renal water transport function and thusly lower ADC values (Namimoto, Yamashita et al. 1999). It has been hypothesized that decreased ADC values noted in kidneys affected by acute renal failure may be due to ischemia and cellular edema (Vexler 1996). The 1999 study (Namimoto, Yamashita et al. 1999) also demonstrated that ADC

values of the renal cortex in kidneys affected by renal artery stenosis were significantly lower than those of normal kidneys, thought to be due to reduced blood perfusion of the affected kidneys.

Functional evaluation of salivary glands using DWI has also been studied. One report noted that the ADC values of the parotid and submandibular salivary glands decreased significantly during the first 5 minutes post salivary stimulation (tablet of ascorbic acid), with an increase in the ADC values noted over the following approximately 20 minutes (Thoeny, De Keyzer et al. 2005). It is proposed that the initial decrease in ADC value is likely due to the release of saliva that is stored within the gland, with the subsequent increase in ADC value possibly associated with active production of new saliva and an increase in the amount of water within the extracellular space (Ferreiro, Prieto et al. 2002).

J. Use of diffusion weighted imaging in the evaluation of lymph nodes (human medicine)

Numerous studies regarding the use of DWI in the differentiation between benign and metastatic lymph nodes have been performed, with somewhat conflicting results. One of the earlier studies was performed in 2003 (Sumi, Noriyuki et al. 2003). This group found that the ADC values of metastatic lymph nodes were significantly higher ($0.41 +/- 0.105 \times 10^{-3} mm^2/s$) versus those of benign (inflammatory) lymph nodes ($0.302 +/- 0.062 \times 10^{-3} mm^2/s$), and also found that nodal lymphomas demonstrated lower ADC values than benign lymph nodes ($0.223 +/- 0.056 \times 10^{-3} mm^2/s$). This study also found that the ADC values of highly or moderately differentiated carcinomas were greater than those of poorly differentiated carcinomas. It was proposed that this finding could be due to the fact that increased nuclear to cytoplasmic ratio and hypercellularity are often associated with poorly differentiated tumors (Sumi, Noriyuki et al. 2003).

A later 2006 study also evaluated the ability of DWI to differentiate causes of

lymphadenopathy (Abdel Razek, Soliman et al. 2006). The findings of this study were

contradictory to the above-mentioned 2003 study, in that the mean ADC value of malignant

lymph nodes was found to be lower (1.09 +/- 0.11 x 10^{-3}mm^2/s) than that of benign lymph nodes

(1.64 +/- 0.16 x 10^{-3}mm^2/s). These findings were corroborated by a later 2009 study, which

found that the mean ADC values of metastatic lymph nodes (squamous cell carcinoma) to be

significantly lower (0.78 +/- 0.09 x 10^{-3}mm^2/s) than those of benign lymph nodes (1.24 +/- 0.16

x 10^{-3}mm^2/s) (Holzapfel, Duetsch et al. 2009). The main difference in the design of the 2003

study versus the design of the 2006 and 2009 studies involved the method for managing necrosis

within evaluated lymph nodes. In the 2003 study (Sumi, Noriyuki et al. 2003), regions of

interest (ROI) were placed manually within each evaluated lymph node on one to four sections

that contained the maximal area of the lymph node, stated to include as much of the nodal

parenchyma as possible. The 2006 study (Abdel Razek, Soliman et al. 2006) first differentiated

between lymph nodes that demonstrated homogeneous signal intensity from those that were

heterogeneously intense. In the homogeneous lymph nodes, ROIs were placed around the

margin of the lymph node. In the heterogeneous lymph nodes, a large ROI was placed in

addition to several smaller ROIs placed within the lymph node. This allowed for separate

calculations of mean ADC values for the hypo- and hyper-intense regions within each lymph

node. Authors reported that the mean ADC value of the solid (hypo-intense) portion of the

heterogeneous lymph nodes was lower than that of the cystic or necrotic (hyperintense) regions

(Abdel Razek, Soliman et al. 2006). The 2009 study (Holzapfel, Duetsch et al. 2009) handled

necrotic regions within evaluated lymph nodes in a similar manner, in that regions of

hyperintensity (on T2-weighted images) were analyzed separately. Holzapfel et al. proposed that

it was likely that the 2003 study determined higher ADC values in metastatic lymph nodes since they included necrotic areas within the ADC measurements, instead of analyzing necrotic regions separately.

A later study sought to compare the ADC values of partially necrotic lymph nodes (Herneth, Mayerhoefer et al. 2010). This study utilized two different ROI settings. Initially, a single ROI containing the whole lymph node was drawn. Then few smaller ROIs were drawn within the lymph node, excluding any necrotic (hyperintense) regions. When comparing these ROI settings, the mean ADC of the lymph nodes when utilizing a single outer ROI was found to be significantly higher (0.92 +/- 0.60 x 10^{-3}mm^2/s) than that found when using multiple smaller ROIs (0.62 +/- 0.14 x 10^{-3}mm^2/s). This group concluded that tissue heterogeneity does influence ADC measurements and therefore recommended evaluation of tissue homogeneity before quantitative analysis (i.e. ADC value measurement) is attempted (Herneth, Mayerhoefer et al. 2010).

In a separate 2010 study, the ability of DWI to differentiate between benign and metastatic pelvic lymph nodes was assessed (Roy, Bierry et al. 2010). The authors reported that all lymph nodes with a short axis diameter greater than 5mm were identifiable on the DWI, but no differences in signal intensity were observed on visual inspection of the DW images. The ADC values were calculated for evaluated lymph nodes by placing elliptical ROIs within each lymph node. This group did not identify a significant difference in the ADC values of the metastatic versus benign lymph nodes, and concluded that although DW images may provide a useful tool in the identification of pelvic lymph nodes, calculation of ADC values does not aide in the differentiation between benign and metastatic disease (Roy, Bierry et al. 2010).

In 2013, a group sought to perform a meta-analysis evaluating the performance of DWI in detecting cervical lymphadenopathy (Wu, Xu et al. 2013). The analysis included eight studies with a total of 229 patients. The conclusions of this meta-analysis included that DWI with ADC value calculation, demonstrates significant differences between benign and malignant cervical lymph nodes, with the ADC value of malignant nodes lower than those of benign (Wu, Xu et al. 2013).

In 2014, a study evaluated the diagnostic performance of DWI in detecting lymph node metastases in a group of patients with bladder and/or prostate cancer (Studer 2014). The study included 4846 lymph nodes, none of which were considered enlarged. Diffusion weighted imaging was performed using three b-values (0, 500, and 1000 s/mm^2). Conventional images were initially read, without inclusion of DW images. During the second reading, DWI were evaluated in addition to conventional MR images. The ADC values were measured for each lymph node via creation of a region of interest. Lymph nodes were classified as suspicious for malignancy if they appeared more intense than groin lymph nodes on DWI and demonstrated hypointensity on ADC. This study found that the ADC values for benign versus malignant lymph nodes did not differ significantly, with mean values of benign lymph nodes found to be 1.009 +/- 0.284 x 10^{-3}mm^2/s, and the malignant group found to be 0.935 +/- 0.178 x 10^{-3}mm^2/s. However, this study did find that combining DWI along with conventional MR imaging improved detection of metastases in normal sized lymph nodes (Studer 2014).

Most recently in 2016, a meta-analysis was performed to evaluate the ability of ADC values to determine lymph node metastasis in cervical cancer (He and Wei 2016). This meta-analysis identified fifteen clinical cohort studies that reported ADC values of lymph nodes in human patients with cervical cancer. This study found that mean ADC value of malignant lymph

nodes was significantly lower than that of benign lymph nodes, however some overlap of ADC values was identified. The authors postulated that this overlap could be due to differences in the degree of tumor invasion/metastasis as well as differences in the degree of inflammatory lymph node hyperplasia (He and Wei 2016).

K. Diffusion weighted imaging in veterinary medicine

Research regarding DWI within veterinary medicine has been primarily regarding the central nervous system, including one study which evaluated the DWI appearance of cerebrovascular accidents in a group of dogs (McConnell, Garosi et al. 2005). This study's findings were similar to those noted in human medicine, where regions of infarction demonstrated focal regions of hyperintensity on DWI that corresponded to regions of hypointensity on the ADC map.

A 2011 study evaluated the ability of ADC values to differentiate between different types of canine intracranial lesions (Sutherland-Smith, King et al. 2011). This group found a variety of mean ADC values within and between groups, with no significant differences in ADC values noted between meningioma, glial tumor, or inflammatory lesions. This group therefore concluded that quantitative ADC values are of limited value in predicting canine intracranial lesion type (Sutherland-Smith, King et al. 2011).

A 2014 study evaluated the regional ADC values of the brain in a group of clinically normal dogs (Hartmann, Soffler et al. 2014).   This group found significant differences in the ADC values for different portions of the brain as well as differences in the ADC values between the right and left cerebral hemispheres.   The authors postulated that differences in regional brain ADC values could be due to differences in myelination, neural density, or fiber orientation

though the reason for the differences between the right and left portions of the brain is not known (Hartmann, Soffler et al. 2014).

Most recently, a 2016 article described the DWI characteristics of the liver in a group of healthy dogs (Del Chicca, Schwarz et al. 2016). This research group found that the mean ADC values of the hepatic parenchyma to be 0.84 +/- 0.17 x 10^{-3}mm^2/s. They also the calculated a mean normalized ADC value for the liver, by dividing the ADC value of the hepatic parenchyma by that of the splenic parenchyma and found this value to be 1.8 +/- 0.4 x 10^{-3}mm^2/s.

Although not necessarily included under the umbrella of veterinary medicine, experimental studies also have been performed for non-central nervous system applications of DWI in various animal models. A 2003 study utilized DWI to evaluate renal function in dogs before and during an ischemic event (renal artery ligation) (Liu and Xie 2003). Calculated ADC values were noted to decrease throughout the renal parenchyma post ligation. After removal of ligation, ADC values of the cortex increased to that of the contralateral (non-ligated) kidney, although ADC values of the medulla remained decreased. This study concluded that DWI could be used as a tool to evaluate renal function following an ischemic event (Liu and Xie 2003).

A 2012 study evaluated the ability of DWI to detect lymph node metastases in rabbits with a VX2 rectal cancer model (Kim, Lee et al. 2012). Images were initially qualitatively assessed for signal intensity on the DW images. Quantitative assessment was then performed via calculation of ADC values for imaged lymph nodes that demonstrated a short-axis diameter of > 3mm, via creation of ROIs within each lymph node. Researchers found that both the metastatic and benign lymph nodes had high signal intensity on the DW images obtained with high b-values, concluding that visual inspection only of lymph nodes on DWI is inaccurate and could possibly lead to overdiagnosis of lymph node metastases. The mean ADC values of metastatic

lymph nodes ($0.96 +/- 0.14 \times 10^{-3}$ mm^2/s) were significantly lower than the benign lymph nodes ($1.51 +/- 0.36 \times 10^{-3}$ mm^2/s). A relatively poor interobserver agreement was identified which was attributed to the reported difficultly experienced when evaluating small (<5mm) lymph nodes on the DW images due to poor signal to noise ratio (Kim, Lee et al. 2012).

A second 2012 study also evaluated the ability of DWI to differentiate between benign and metastatic lymph nodes in a rabbit model (Wang, Liao et al. 2012). This study evaluated axillary lymph nodes in rabbits injected either with adjuvant only or with VX2 tumor tissue suspension. Any axillary lymph nodes with a short axis diameter equal or greater than 5mm were included in the study. An ROI was created within each lymph node to calculate an ADC value for each node. This group also drew an ROI of similar size within muscle at the same level of each lymph node in order to calculate a relative ADC value (rADC) using the equation: rADC = ADC (lymph node) / ADC (muscle). Similar to the prior study, this group found that the mean rADC value of the benign lymph nodes ($0.9 +/- 0.14 \times 10^{-3}$ mm^2/s) was significantly higher than that of the metastatic group ($0.7 +/- 0.18 \times 10^{-3}$ mm^2/s) (Wang, Liao et al. 2012).

CHAPTER 2: DIFFUSION WEIGHTED IMAGING IN THE DIFFERENTIATION BETWEEN
BENIGN AND METASTATIC LYMPH NODES IN CANINE PATIENTS WITH HEAD AND
NECK DISEASE

A. Introduction

Factors listed by the World Health Organization that may be used to determine neoplastic
disease stage include the size of the tumor, evidence of distant metastasis, and regional lymph
node involvement (Owen 1980). Although morphologic imaging techniques (such as CT or MR
imaging) allow for the detection of enlarged lymph nodes, definitive differentiation between
benign and metastatic lymph nodes cannot be made. Metabolic imaging with photon emission
tomography (PET) can aid in this differentiation, however, this method utilizes ionizing radiation
and is not readily accessible to most veterinary patients. Lymph node size alone has been
suggested to be insufficient for accurate clinical staging of diseases such as oral melanoma, with
cytologic or histologic examination of the regional lymph nodes recommended (Williams and
Packer 2003). Regional lymph nodes that receive efferent lymph from the canine head and neck
include the mandibular and medial retropharyngeal lymph nodes (MRPLN). The MRPLN have
been considered difficult to evaluate by fine-needle aspiration (Smith 1995). Therefore, a non-
invasive, non-ionizing method for accurate differentiation of metastatic from benign lymph
nodes would be a particularly useful technique for the staging of canine head and neck neoplasia.
Diffusion weighted magnetic imaging (DWI) could potentially provide such an imaging method.

Diffusion weighted imaging is a form of magnetic resonance imaging that utilizes the
diffusion of water molecules to create image contrast. Tissues that demonstrate restricted
diffusion (such as solid neoplastic tissue) will contain water molecules that remain static during

the acquisition of the DW sequence, which will result in no significant change in signal intensity. Tissues that demonstrate free diffusion (such as cystic tissue) will possess moving water molecules that are not in the same place during the DWI acquisition. This water motion will result in attenuation of the MR signal, with the degree of water motion proportional to the degree of signal attenuation (Koh and Collins 2007). Once DW images are obtained, a second type of magnetic resonance image termed an apparent diffusion coefficient (ADC) can be created. This ADC image represents a quantitative expression of water motion. By creating regions of interest (ROI) within these ADC images, ADC values can be determined for particular structures, including lymph nodes.

The ability of DWI to differentiate between metastatic and benign lymph nodes has been demonstrated in human clinical studies as well as several experimental studies in animal models (Abdel Razek, Soliman et al. 2006) (Wu, Xu et al. 2013) (He and Wei 2016) (Wang, Liao et al. 2012). To the authors' knowledge, no studies have described the application of this technique in dogs with naturally occurring disease. The objective of this exploratory study was to evaluate DWI and ADC as potential future methods for detecting metastatic lymph nodes in dogs with naturally occurring disease. We hypothesized that that DWI and ADC methods previously developed for use in humans could be modified for use in dogs and that characteristics identified with these methods would differ for benign versus metastatic lymph nodes in a sample of canine patients with head or neck disease metastatic and that the metastatic lymph nodes will have a significantly different mean ADC value than that of the benign lymph nodes.

B. Materials and methods

a. Subjects:

This study was a prospective exploratory experimental design. Client-owned canine patients with head and neck disease were recruited during a period from July 2014 to March 2016. The Institutional Animal Care and Use Committee of the Virginia Maryland Regional College of Veterinary Medicine approved the study protocol (IACUC #14-049). Dogs were included in the study if they had at least one enlarged mandibular or MRPLN and if clients agreed to allow cytologic and histologic confirmation of lymph node pathology. An enlarged lymph node was defined as a lymph node deemed subjectively enlarged by one of our institution's two board certified veterinary oncologists and measured at least 1.5cm in one dimension. Exclusion criteria were any condition that could make the patient a poor anesthetic candidate, previous fine needle aspirate or biopsy of the enlarged lymph node, or client refusal to allow lymph node cytology and biopsy.

b. MR imaging techniques:

With informed client consent, patients meeting inclusion criteria were placed under general anesthesia using anesthetic protocols approved by the institution's board certified veterinary anesthesiologists. The precise anesthetic protocols differed for each dog. All imaging was performed by the same imaging technologist, using the same in-house 1.5T scanner (Intera, Philips Healthcare, Eindhoven, Netherlands) and Q-body coil. Each patient was placed in dorsal recumbency for image acquisition. Pulse sequences included STIR (dorsal, transverse), T2-weighted and T1-weighted fast spin echo (dorsal, transverse), and T1-weighted images post intravenous bolus administration of gadopentetate dimeglumine (Magnevist (0.1 mL/kg)) (dorsal, transverse, sagittal). Prior to contrast administration, DW images with inherent STIR

were obtained in the transverse plane, without the use of respiratory gating. These DW images

were acquired using a multislice, single-shot, inversion recovery, echo planar imaging sequence,

using two b-values (0, 1000 s/mm^2). ADC images were then created using the formula: ADC =

(1/ b_2 – b_1) ln(SI_1/SI_2) (**Equation 2)**. An effort was made to match slice locations for the T2-

weighted and ADC images as much as possible, but the sequences were not co-registered. Scan

parameters were as follows: T2-weighted (SE): repetition time (TR) = 6254 to 7697 ms, echo

time (TE) = 110 ms, number of acquisitions (NEX) = 4, slice thickness = 5mm, interslice gap =

0.5mm, field of view (FOV) = 176 to 320 x 176 x320, matrix = 172 to 232 x 165 to 230; STIR:

TR = 2265 to 2472 ms, TE = 30 ms, TI = 140 ms, NEX = 2, slice thickness = 5mm, interslice

gap = 0.5mm, field of view (FOV) = 160 to 288 x 160 to 288, matrix = 156 to 192 x 122 to 153;

T1-weighted (SE): TR = 500 to 558ms, TE = 7 ms. NEX = 3, slice thickness = 5mm, interslice

gap = 0.5mm, field of view (FOV) = 224 to 320 x 224 to 320, matrix = 192 to 268 x 192 to 268;

DWI: TR = 9764 to 12730 ms, TE = 72 ms, slice thickness = 5mm, interslice gap = -1 to 0mm,

field of view (FOV) = 80 to 112 x 80 to 112, matrix = 64 to 84 x 67 to 85.

c. *Lymph node assessment techniques:*

Immediately following image acquisition, patients were maintained under general

anesthesia so that Tru-cut biopsy samples (18G) of any lymph node deemed enlarged could be

obtained using ultrasound guidance. Additionally, fine needle aspirate samples (22G) of any

accessible non-enlarged mandibular or MRPLN were obtained using ultrasound guidance. A

board certified veterinary pathologist who was unaware of the patient's imaging findings

reviewed all obtained tissue samples. Based on the pathologist's evaluation, each sampled

lymph node was then placed into one of two categories: metastatic or benign, with both normal

and inflammatory lymph nodes included in the benign group.

d. *Image analysis:*

All MR images were stored on a Picture Archiving and Communication System (PACS, Sound Fusion, Carlsbad, CA), and displayed on a dedicated diagnostic workstation computer. Four observers independently traced regions of interest (ROI) and calculated ADC values for each lymph node: a board-certified veterinary radiologist, a board-certified veterinary neurologist, a board-certified veterinary oncologist, and a third year diagnostic imaging resident. Patient information was rendered anonymous for images that were provided to observers to help minimize bias. The first three observers were unaware of the diagnosis of the subjects' head or neck disease and the fourth observer was aware of the diagnosis at the time of the calculations. A free hand ROI drawing tool (Osirix imaging processor) was used to encompass as much of every sampled lymph node as possible, with ROIs drawn on every slice that contained visible lymph node. If a large area of suspected necrosis was identified based on STIR hyperintensity and lack of contrast enhancement, observers were instructed to exclude that area from ROI tracings. For each image slice depicting the lymph node of interest, the ROI was first drawn on the T2-weighted transverse images, and then copied and pasted onto the corresponding ADC map image (**Fig. 1**). Because the MR images were not co-registered, each observer was allowed to move the ROI (without alteration of the ROI shape or size) to their satisfaction, using the linguofacial veins as reference. A mean ADC value (mm^2/s) was recorded for each ROI.

The three observers who were unaware of the diagnosis of each subjects' head or neck disease, subjectively graded each sampled lymph node on a scale of zero to five: 0 = normal, 1 = abnormal, definitely benign, 2 = abnormal, likely benign, 3 = abnormal, unsure if benign or metastatic, 4 = abnormal, likely metastatic, and 5 = abnormal, definitely metastatic. Two observers (one blinded and one aware of the diagnoses of the subjects' head or neck disease) also

came to a consensus regarding the qualitative characteristics of the enlarged lymph nodes on the DWI and ADC sequences. These two observers identified each enlarged lymph node as hypointense, isointense, or hyperintense relative to the mandibular salivary glands. Initially, it was planned to additionally assess the heterogeneity of each enlarged lymph node, but this criterion was eliminated due to poor overall spatial resolution of the DWI and ADC sequences was deemed too poor for this assessment.

e. *Statistical analysis:*

Normal probability plots showed that ADC values followed a normal distribution. Subsequently, a mixed model analysis of variance (ANOVA) was used to compare the means of the ADC values between the two groups of lymph nodes (benign vs. metastatic) and to assess the effects of observer. The linear model specified group, observer, and the interaction between group and observer as fixed effects with Kenward-Roger approximation as the denominator degrees of freedom. Random effects included dog, lymph node within dog, and slice within both dog and lymph node. To specifically compare groups within each observer and to compare observers within each group, the interaction between group and observer was sliced by the Slicediff option of the SAS procedure Proc Glimmix. Where appropriate, P-values were adjusted for multiple comparisons using Tukey's procedure. Inter-observer variability was assessed using coefficient of variation. Normal probability plots showed the coefficients of variation followed a normal distribution. A mixed model ANOVA was also used to compare inter-observer coefficients of variation between groups of lymph nodes (benign vs. metastatic). The linear model specified group as the fixed effect with Kenward-Roger approximation as the denominator degrees of freedom. Dog and lymph node within dog were the random effects. Proportions of truly benign lymph nodes that were subjectively classified as benign and proportions of truly

34

metastatic lymph nodes that were subjectively classified as metastatic were generated as simple measures of agreement between subjective visual assessment score and pathologist characterization (metastatic vs. benign). Statistical significance was set to a P-value less than 0.05. All analyses were performed using SAS version 9.4 (Cary, NC, USA).

C. Results

Our study population consisted of 8 client owned canine patients. The ages of the subjects ranged from 9 to 11years (mean: 10yr). There were four castrated males and four spayed females. Breeds of the subjects included: Rottweiler (1), Gordon Setter (1), Chesapeake Bay Retriever (1), Labrador Retriever (1), Staffordshire Terrier (1), and mixed breed (3). The etiologies of the subjects' head and neck disease included: oral melanoma (4), nasal tumors (2), basaloid apocrine gland adenocarcinoma (1), and pyogranulomatous/lymphoplasmacytic inflammation (1).

A total of twenty lymph nodes were sampled (6 metastatic, 14 benign). Ten of these lymph nodes were deemed enlarged upon palpation by an oncologist (6 metastatic, 4 benign) (Table 1). The qualitative characteristics of the enlarged lymph nodes on the ADC sequence were as follows: 3 of 6 (50%) of the metastatic lymph nodes were isointense (versus the mandibular salivary glands), 1 of 6 (17%) of the metastatic lymph nodes was hypointense, 1 of 6 (17%) of the metastatic lymph nodes was iso- to hyperintense, and 1 of 6 (17%) of the metastatic lymph nodes was iso- to hypointense; 2 of 4 (50%) benign lymph nodes were iso- to hyperintense, and 2 of 4 (50%) benign lymph nodes were isointense (Table 2). Regarding the appearance of the enlarged lymph nodes on the DWI sequence: 3 of 6 (50%) metastatic lymph nodes were isointense, 1 of 6 (17%) metastatic lymph nodes was iso- to hyperintense, 1 of 6 (17%) metastatic lymph nodes was hypointense, 1 of 6 (17%) metastatic lymph nodes was

hyperintense, 2 of 4 (50%) benign lymph nodes were iso- to hyperintense and 2 of 4 (50%) benign lymph nodes were hyperintense,

The mean ADC value of the metastatic lymph nodes was $(0.663 +/- 0.310)$ x $10^{-3}mm^2/s$, with values ranging from (0.034) x $10^{-3}mm^2/s$ to (1.22) x $10^{-3}mm^2/s$. The mean ADC value of the benign lymph nodes was $(0.933 +/- 0.215)$ x $10^{-3}mm^2/s$, with values ranging from (0.175) x $10^{-3}mm^2/s$ to (1.38) x $10^{-3}mm^2/s$ (Fig 2). The difference between these mean ADC values approached significance, (P-value of 0.0566). The mean ADC values of the metastatic (M) and benign (B) lymph nodes for each observer were: observer 1 (M: $(0.619 +/- 0.330)$ x $10^{-3}mm^2/s$, B: $(0.917 +/- 0.217)$ x $10^{-3}mm^2/s$), observer 2 (M: $(0.661 +/- 0.279)$ x $10^{-3}mm^2/s$, B: $(0.922 +/- 0.219)$ x $10^{-3}mm^2/s$), observer 3 (M: $(0.719 +/- 0.331)$ x $10^{-3}mm^2/s$, B: $(0.948 +/- 0.233)$ x $10^{-3}mm^2/s$), and observer 4 (M: $(0.652 +/- 0.305)$ x $10^{-3}mm^2/s$, B: $(0.944 +/- 0.195)$ x $10^{-3}mm^2/s$) (Fig 3). A significant difference between the mean ADC values of the benign and metastatic lymph nodes were identified by two of the observers: observer 1 P-value: 0.0308, observer 2 P-value: 0.0775, observer 3 P-value: 0.1603, and observer 4 P-value: 0.0368.

The mean ADC value of the metastatic lymph nodes (which were all enlarged) was $(0.663 +/- 0.310)$ x $10^{-3}mm^2/s$, with values ranging from 0.034 x $10^{-3}mm^2/s$ to 1.22 x $10^{-3}mm^2/s$. The mean ADC of the enlarged benign lymph nodes was $(0.974 +/- 0.151)$ x $10^{-3}mm^2/s$, with values ranging from 0.635 x $10^{-3}mm^2/s$ to 1.26 x $10^{-3}mm^2/s$ (Fig 4). A significant difference between the mean ADC values of the enlarged benign and metastatic lymph nodes was not identified, (P-value: 0.2466). The mean ADC values of the metastatic (M) and enlarged benign (B) lymph nodes for each observer were: observer 1 (M: $(0.619 +/- 0.330)$ x $10^{-3}mm^2/s$, B: $(0.961 +/- 0.140)$ x $10^{-3}mm^2/s$), observer 2 (M: $(0.661 +/- 0.279)$ x $10^{-3}mm^2/s$, B: $(0.960 +/- 0.133$ x $10^{-3}mm^2/s$), observer 3 (M: $(0.719 +/- 0.331)$ x $10^{-3}mm^2/s$, B: $(0.987 +/- 0.190)$ x 10^{-}

^{3}mm^2/s), and observer 4 (M: $(0.652 +/- 0.305)$ x 10^{-3}mm^2/s, B: $(0.989 +/- 0.144)$ x 10^{-3}mm^2/s) (Fig 5). A significant difference between the mean ADC values of the enlarged benign and metastatic lymph nodes was not identified by any of the observers: observer 1 P-value: 0.1985, observer 2 P-value: 0.2349, observer 3 P-value: 0.3442, and observer 4 P-value: 0.2055.

The inter-observer coefficient of variation for benign lymph nodes was 10.39%, with the confidence interval from 1.96% to 18.81%. The inter-observer coefficient of variation for the metastatic lymph nodes was 15.88%, with the confidence interval from 6.99% to 24.77% (Table 3). Inter-observer variability was not significantly different between the metastatic and benign lymph nodes (P-value: 0.2303).

With regards to the observers' visual subjective assessment and scoring of the sampled lymph nodes, numeric categorizations 0, 1, or 2 were considered as an assessment of benign (B), categorization of 3 was considered benign/metastatic (M/B) and categorizations of 4 or 5 were considered as an assessment of metastatic (M). Observers correctly identified 33 of 42 (78.6%) of benign lymph nodes as benign; correctly identified 8 of 18 (44.4%) of metastatic lymph nodes as metastatic; incorrectly identified 4 of 42 (9.5%) of benign lymph nodes as metastatic; incorrectly identified 8 of 18 (44.4%) of metastatic lymph nodes as benign; identified 5 of 42 (11.9%) benign lymph nodes as M/B; and identified 2 of 18 (11.1%) of metastatic lymph nodes as M/B (Table 4).

D. Discussion

Regional lymph node involvement is an important factor in tumor staging (Owen 1980), and may impact prognosis as well as therapeutic planning. DWI is a non-invasive imaging technique that does not utilize ionizing radiation and does not require administration of a contrast agent. Our proof of concept study evaluated the ability of DWI to differentiate between benign

and metastatic regional lymph nodes in a group of canine patients with naturally head or neck disease.

Two of our study's observers identified a significant difference between the mean ADC values of metastatic and benign (enlarged and normal sized) lymph nodes, which was in accordance with several human clinical studies (Abdel Razek, Soliman et al. 2006) (Holzapfel, Duetsch et al. 2009) (He and Wei 2016). However, the other two observers in our study did not identify a significant difference, which was also in accordance with another previous human study (Roy, Bierry et al. 2010). When the values from all observers were pooled, the difference between the mean ADC values of all benign and metastatic lymph nodes approached significance (P-value: 0.0566). No significant difference was identified between the ADC values of the metastatic and enlarged benign lymph nodes for any observer, or when all observers' values were pooled. There was substantial overlap noted in the ADC values of the benign and metastatic lymph nodes.

Other studies have identified significant overlap between the ADC values of benign and metastatic lymph nodes, which could lead to false-negative or false positive identifications using DWI (Park, Kim et al. 2009). One reason for the overlap of ADC values between the benign and metastatic lymph nodes in our study could be the fact that lower ADC values are not specific for neoplastic cells, as other conditions such as ischemia can also reduce tissue diffusivity (Park, Kim et al. 2009). The presence of fibrous tissue may also create regions of restricted diffusion, which could lead to a lower ADC value for a given lymph node (Roy, Bierry et al. 2010). Conversely, metastatic lymph nodes could demonstrate increased ADC values if they contain cystic or necrotic regions that were not excluded from the ROI analysis. Additionally, a metastatic lymph node may not be entirely encompassed by neoplastic cells, so that a single

lymph node could contain both benign and metastatic regions, leading to various ADC values (Choi, Kim et al. 2009). Because of this possibility, it has been proposed that the minimum ADC value within an ROI drawn within a lymph node could serve as a better representative of node status than the mean ADC value (Choi, Kim et al. 2009).

Another possible cause of ADC value variability could be due to inter-observer variability. A 2015 study identified inter-observer variability as the largest source of error (up to 37%) in ADC measurements (normal and malignant breast tissue)(Giannotti, Waugh et al. 2015). This group suggested that in follow-up clinical or research studies, where possible only one observer should measure serial ADC values in any one patient (Giannotti, Waugh et al. 2015). In our study, the inter-observer coefficient of variation was greater than 10% (the acceptable level) for both the benign and metastatic lymph nodes. Perhaps group training (with all observers present) as well as formal assessment of intra-observer repeatability could help improve inter-observer variability and could aid in creating a standardized (possibly multi-institutional) approach for evaluating ADC values.

A 2008 multi-institutional study evaluated whether ADC values vary between imagers, vendors, field strengths, and intra-imager conditions (Sasaki, Yamada et al. 2008). This group compared the ADC values calculated from 10 different MR scanners, 4 different vendors, and two different field strengths all using the same subjects. ADC values were calculated using hand drawn ROIs within the frontal white matter and thalamus of 12 healthy human volunteers. They concluded that ADC values can vary significantly between scanners, vendors, and field strengths (Sasaki, Yamada et al. 2008), a finding which must be kept in mind with respect to future studies that may be multi-institutional. In an attempt to normalize ADC values, it has been suggested that a relative apparent diffusion coefficient (rADC) be calculated, (rADC = ADC_{lesion}

/ADC$_{\text{reference site.}}$), with these rADC values possibly improving the accuracy for differentiating

metastatic from non-metastatic lymph nodes (Park, Kim et al. 2009). Additionally, the use of a

phantom that could be transported to different institutions could be used to assess ADC

measurement variability and minimize protocol differences, as demonstrated in a recent 2016

study, (Keenan, Peskin et al. 2016).

In our study, the majority of the enlarged metastatic lymph nodes (5 of 6) were

considered either hypointense (1), hypointense to isointense (1), or isointense (3), relative to the

mandibular salivary glands, whereas, the enlarged benign lymph nodes were considered either

isointense (2 of 4) or isointense to hyperintense (2 of 4). This finding could be representative of

a trend towards a lower mean ADC value (represented by hypointensity) of the metastatic lymph

nodes versus that of the benign, although larger subject numbers are necessary to identify any

significant associations.

Our study had several limitations, the first being our low subject number, with a total of

only 8 dogs with 10 enlarged (6 metastatic, 4 benign) lymph nodes. A second limitation is that

our study utilized only two b-values (0, 1000 s/mm^2). A b-value of 0 s/mm^2 can be affected by

perfusion effects, however, it has been reported that lymph nodes do not generally have a large

amount of perfusion, and therefore perfusion effects should not have had a large impact on the

ADC values of lymph nodes (Choi, Kim et al. 2009). However with the acquisition of additional

b-values, the effect of image noise may be reduced, and would enable calculation of perfusion-

insensitive ADC values by excluding the b-value of 0 s/mm^2 from the ADC calculation (Padhani,

Liu et al. 2009). Another limitation of our study was that the MR images were not co-registered.

The ROI drawn on the T2-weighted transverse sequence was copied and pasted on the ADC

sequence, after which the ROI at times did not perfectly align to the position of the evaluated

lymph node. The observers in our study were then allowed to move the ROI (without adjusting the ROI size or shape), which certainly created a source of error and variability for our measurements. Our study also did not limit the type of our subjects' head or neck disease to one disease process. The included different histologic subtypes may each have had differences in ADC values due to the differences in cellular architecture. Finally, the sampling method used for lymph node characterization (fine needle aspirate or biopsy) could have obtained a sample that was not representative of the entire lymph node, which could have lead to an incorrect characterization of that lymph node.

CHAPTER 3: CONCLUSIONS AND FURTHER RESEARCH

In summary, only two of four observers identified a significant difference between the mean ADC values of benign and metastatic lymph nodes, and when the data from all of the observers were pooled, the difference between the mean ADC values of the benign and metastatic approached but did not reach significance. Therefore our hypothesis was not supported. However, our data does show promise that DWI may be used to differentiate between benign and metastatic lymph nodes. Accordingly, the main conclusion of our study is that future studies regarding the use of DWI for lymph node characterization in veterinary medicine are warranted. With future studies evaluating increased numbers of veterinary patients, conclusions may be drawn regarding the use of DWI as a non-invasive method of lymph node characterization that does not utilize ionizing radiation. Additionally with future research, DWI may also provide a useful tool for staging tumors (leading to improved prediction of expected outcome and more appropriate treatment recommendations), as well as provide a novel method to monitor therapeutic response.

References:

Abdel Razek, A. A., G. Gaballa, G. Elhawarey, A. S. Megahed, M. Hafez and N. Nada (2009). "Characterization of pediatric head and neck masses with diffusion-weighted MR imaging." Eur Radiol **19**(1): 201-208.

Abdel Razek, A. A., N. Y. Soliman, S. Elkhamary, M. K. Alsharaway and A. Tawfik (2006). "Role of diffusion-weighted MR imaging in cervical lymphadenopathy." Eur Radiol **16**(7): 1468-1477.

Ballegeer, E. A., W. M. Adams, R. R. Dubielzig, M. C. Paoloni, J. M. Klauer and N. S. Keuler (2010). "Computed tomography characteristics of canine tracheobronchial lymph node metastasis." Vet Radiol Ultrasound **51**(4): 397-403.

Bammer, R. (2003). "Basic principles of diffusion-weighted imaging." European Journal of Radiology **45**: 169-184.

Basser, P. J., J. Mattiello and D. LeBihan (1994). "Estimation of the effective self-diffusion tensor from the NMR spin echo." J Magn Reson B **103**(3): 247-254.

Benveniste, H., L. W. Hedlund and G. A. Johnson (1992). "Mechanism of detection of acute cerebral ischemia in rats by diffusion-weighted magnetic resonance microscopy." Stroke **23**(5): 746-754.

Benzuidenhout, A. J. (2013). The lymphatic system. In: Miller's Anatomy of the Dog . St. Louis, Missouri, Elsevier.

Bitar, R., G. Leung, R. Perng, S. Tadros, A. R. Moody, J. Sarrazin, C. McGregor, M. Christakis, S. Symons, A. Nelson and T. P. Roberts (2006). "MR pulse sequences: what every radiologist wants to know but is afraid to ask." Radiographics **26**(2): 513-537.

Burns, G. O., P. V. Scrivani, M. S. Thompson and H. N. Erb (2008). "Relation between age, body weight, and medial retropharyngeal lymph node size in apparently healthy dogs." Vet Radiol Ultrasound **49**(3): 277-281.

Casteleyn, C. R., M. van der Steen, J. Declercq and P. Simoens (2008). "The buccal lymph node (lymphonodus buccalis) in dogs: occurrence, anatomical location, histological characteristics and clinical implications." Vet J **175**(3): 379-383.

Choi, E. K., J. K. Kim, H. J. Choi, S. H. Park, B. W. Park, N. Kim, J. S. Kim, K. C. Im, G. Cho and K. S. Cho (2009). "Node-by-node correlation between MR and PET/CT in patients with uterine cervical cancer: diffusion-weighted imaging versus size-based criteria on T2WI." Eur Radiol **19**(8): 2024-2032.

Choi, M. Y., J. W. Lee and K. J. Jang (1995). "Distinction between benign and malignant causes of cervical, axillary, and inguinal lymphadenopathy: value of Doppler spectral waveform analysis." AJR Am J Roentgenol **165**(4): 981-984.

Chong, V. F., Y. F. Fan and J. B. Khoo (1996). "MRI features of cervical nodal necrosis in metastatic disease." Clin Radiol **51**(2): 103-109.

Cohen, M., M. W. Bohling, J. C. Wright, E. A. Welles and J. S. Spano (2003). "Evaluation of sensitivity and specificity of cytologic examination: 269 cases (1999-2000)." J Am Vet Med Assoc **222**(7): 964-967.

Cowell, R. L., K. E. Dorsey and J. H. Meinkoth (2003). "Lymph node cytology." Vet Clin North Am Small Anim Pract **33**(1): 47-67, v.

Cowell, R. L., Tyler, R. D., Meinkoth, J. H., DeNicola, D. B. (2008). Diagnostic cytology and hematology of the dog and cat. St. Louis, Missouri, Mosby Elsevier.

De Swarte, M., K. Alexander, B. Rannou, M. A. D'Anjou, L. Blond and G. Beauchamp (2011). "Comparison of sonographic features of benign and neoplastic deep lymph nodes in dogs." Vet Radiol Ultrasound **52**(4): 451-456.

Del Chicca, F., A. Schwarz, P. Grest and P. R. Kircher (2016). "Perfusion- and diffusion-weighted magnetic resonance imaging of the liver of healthy dogs." Am J Vet Res **77**(5): 463-470.

Doi, H., N. Beppu, T. Kato, M. Noda, H. Yanagi, N. Tomita, N. Kamikonya and S. Hirota (2015). "Diffusion-weighted magnetic resonance imaging for prediction of tumor response to neoadjuvant chemoradiotherapy using irinotecan plus S-1 for rectal cancer." Mol Clin Oncol **3**(5): 1129-1134.

Ferreiro, M. C., M. H. Prieto, S. B. Rodriguez, R. L. Vazquez, A. C. Iglesias and P. D. Dios (2002). "Whole stimulated salivary flow in patients with chronic hepatitis C virus infection." J Oral Pathol Med **31**(2): 117-120.

Fry, M. M., McGavin M. D. (2012). Bone Marrow, Blood Cells, and the Lymphatic System. In: Pathologic Basis of Veterinary Disease. St. Louis, Missouri
, Elsevier.

Giannotti, E., S. Waugh, L. Priba, Z. Davis, E. Crowe and S. Vinnicombe (2015). "Assessment and quantification of sources of variability in breast apparent diffusion coefficient (ADC) measurements at diffusion weighted imaging." Eur J Radiol **84**(9): 1729-1736.

Guo, Y., C. You-Quan, C. Zu-Long, G. Yuan-Gui, A. Ning-Yu, M. Lin, M. Srikanth and G. Jia-Hong (2002). "Differentiation of Clinically Benign and Malignant Breast Lesions Using Diffusion-Weighted Imaging." Journal of Magnetic Resonance Imaging **16**: 172-178.

Hagmann, P., L. Jonasson, P. Maeder, J. P. Thiran, V. J. Wedeen and R. Meuli (2006). "Understanding diffusion MR imaging techniques: from scalar diffusion-weighted imaging to diffusion tensor imaging and beyond." Radiographics **26 Suppl 1**: S205-223.

Haig, D. M., J. Hopkins and H. R. Miller (1999). "Local immune responses in afferent and efferent lymph." Immunology **96**(2): 155-163.

Hannoun, S., F. Durand-Dubief, C. Confavreux, D. Ibarrola, N. Streichenberger, F. Cotton, C. R. Guttmann and D. Sappey-Marinier (2012). "Diffusion tensor-MRI evidence for extra-axonal neuronal degeneration in caudate and thalamic nuclei of patients with multiple sclerosis." AJNR Am J Neuroradiol **33**(7): 1363-1368.

Hartmann, A., C. Soffler, K. Failing, A. Schaubmar, M. Kramer and M. J. Schmidt (2014). "Diffusion-weighted magnetic resonance imaging of the normal canine brain." Vet Radiol Ultrasound **55**(6): 592-598.

He, X. Q. and L. N. Wei (2016). "Diagnostic value of lymph node metastasis by diffusion-weighted magnetic resonance imaging in cervical cancer." J Cancer Res Ther **12**(1): 77-83.

Herneth, A. M., M. Mayerhoefer, R. Schernthaner, A. Ba-Ssalamah, C. Czerny and J. Fruehwald-Pallamar (2010). "Diffusion weighted imaging: lymph nodes." Eur J Radiol **76**(3): 398-406.

Hillers, K. R., W. S. Dernell, M. H. Lafferty, S. J. Withrow and S. E. Lana (2005). "Incidence and prognostic importance of lymph node metastases in dogs with appendicular osteosarcoma: 228 cases (1986-2003)." J Am Vet Med Assoc **226**(8): 1364-1367.

Hiwatashi, A., T. Kinoshita, T. Moritani, H. Z. Wang, D. A. Shrier, Y. Numaguchi, S. E. Ekholm and P. L. Westesson (2003). "Hypointensity on diffusion-weighted MRI of the brain related to T2 shortening and susceptibility effects." AJR Am J Roentgenol **181**(6): 1705-1709.

Hoang, J. K., J. Vanka, B. J. Ludwig and C. M. Glastonbury (2013). "Evaluation of cervical lymph nodes in head and neck cancer with CT and MRI: tips, traps, and a systematic approach." <u>AJR Am J Roentgenol</u> **200**(1): W17-25.

Holzapfel, K., S. Duetsch, C. Fauser, M. Eiber, E. J. Rummeny and J. Gaa (2009). "Value of diffusion-weighted MR imaging in the differentiation between benign and malignant cervical lymph nodes." <u>Eur J Radiol</u> **72**(3): 381-387.

Issa, B. (2002). "In vivo measurement of the apparent diffusion coefficient in normal and malignant prostatic tissues using echo-planar imaging." <u>J Magn Reson Imaging</u> **16**(2): 196-200.

Johnson, P. J., R. Elders, P. Pey and R. Dennis (2015). "Clinical and Magnetic Resonance Imaging Features of Inflammatory Versus Neoplastic Medial Retropharyngeal Lymph Node Mass Lesions in Dogs and Cats." <u>Vet Radiol Ultrasound</u>.

Keenan, K. E., A. P. Peskin, L. J. Wilmes, S. O. Aliu, E. F. Jones, W. Li, J. Kornak, D. C. Newitt and N. M. Hylton (2016). "Variability and bias assessment in breast ADC measurement across multiple systems." <u>J Magn Reson Imaging</u>.

Kim, S. H., J. M. Lee, S. K. Moon, Y. E. Chung, J. H. Paik, S. H. Choi, M. U. Kim, J. K. Han and B. I. Choi (2012). "Evaluation of lymph node metastases: comparison of gadofluorine M-enhanced MRI and diffusion-weighted MRI in a rabbit VX2 rectal cancer model." <u>J Magn Reson Imaging</u> **35**(5): 1179-1186.

Kim, Y. C., J. S. Lim, K. C. Keum, K. A. Kim, S. Myoung, S. J. Shin, M. J. Kim, N. K. Kim, J. Suh and K. W. Kim (2011). "Comparison of diffusion-weighted MRI and MR volumetry in the evaluation of early treatment outcomes after preoperative chemoradiotherapy for locally advanced rectal cancer." <u>J Magn Reson Imaging</u> **34**(3): 570-576.

Kinns, J. and W. Mai (2007). "Association between malignancy and sonographic heterogeneity in canine and feline abdominal lymph nodes." <u>Vet Radiol Ultrasound</u> **48**(6): 565-569.

Kneissl, S. and A. Probst (2006). "Magnetic resonance imaging features of presumed normal head and neck lymph nodes in dogs." <u>Vet Radiol Ultrasound</u> **47**(6): 538-541.

Kneissl, S. and A. Probst (2007). "Comparison of computed tomographic images of normal cranial and upper cervical lymph nodes with corresponding E12 plastinated-embedded sections in the dog." <u>Vet J</u> **174**(2): 435-438.

Koh, D. M. and D. J. Collins (2007). "Diffusion-weighted MRI in the body: applications and challenges in oncology." <u>AJR Am J Roentgenol</u> **188**(6): 1622-1635.

Kwee, T. C., T. Takahara, O. Reiji, N. R. A. J. and L. P. R. (2008). "Diffusion-weighted whole-body imaging with background body signal suppression (DWIBS): features and potential applications in oncology." <u>Eur Radiol</u> **18**: 1937-1952.

Kyzas, P. A., E. Evangelou, D. Denaxa-Kyza and J. P. Ioannidis (2008). "18F-fluorodeoxyglucose positron emission tomography to evaluate cervical node metastases in patients with head and neck squamous cell carcinoma: a meta-analysis." <u>J Natl Cancer Inst</u> **100**(10): 712-720.

Lang, P., M. F. Wendland, M. Saeed, A. Gindele, W. Rosenau, A. Mathur, C. A. Gooding and H. K. Genant (1998). "Osteogenic sarcoma: noninvasive in vivo assessment of tumor necrosis with diffusion-weighted MR imaging." <u>Radiology</u> **206**(1): 227-235.

Langenbach, A., P. M. McManus, M. J. Hendrick, F. S. Shofer and K. U. Sorenmo (2001). "Sensitivity and specificity of methods of assessing the regional lymph nodes for evidence of metastasis in dogs and cats with solid tumors." <u>J Am Vet Med Assoc</u> **218**(9): 1424-1428.

Lansberg, M. G., A. M. Norbash, M. P. Marks, D. C. Tong, M. E. Moseley and G. W. Albers (2000). "Advantages of adding diffusion-weighted magnetic resonance imaging to conventional magnetic resonance imaging for evaluating acute stroke." Arch Neurol **57**(9): 1311-1316.

Le Bihan, D. (2008). "Intravoxel incoherent motion perfusion MR imaging: a wake-up call." Radiology **249**(3): 748-752.

Le Bihan, D., E. Breton, D. Lallemand, P. Grenier, E. Cabanis and M. Laval-Jeantet (1986). "MR imaging of intravoxel incoherent motions: application to diffusion and perfusion in neurologic disorders." Radiology **161**(2): 401-407.

Le Bihan, D., R. Turner and J. R. MacFall (1989). "Effects of intravoxel incoherent motions (IVIM) in steady-state free precession (SSFP) imaging: application to molecular diffusion imaging." Magn Reson Med **10**(3): 324-337.

LeBlanc, A. K., B. W. Jakoby, D. W. Townsend and G. B. Daniel (2009). "18FDG-PET imaging in canine lymphoma and cutaneous mast cell tumor." Vet Radiol Ultrasound **50**(2): 215-223.

Liu, A. S. and J. X. Xie (2003). "Functional evaluation of normothermic ischemia and reperfusion injury in dog kidney by combining MR diffusion-weighted imaging and Gd-DTPA enhanced first-pass perfusion." J Magn Reson Imaging **17**(6): 683-693.

Luciani, A., A. Vignaud, M. Cavet, J. T. Nhieu, A. Mallat, L. Ruel, A. Laurent, J. F. Deux, P. Brugieres and A. Rahmouni (2008). "Liver cirrhosis: intravoxel incoherent motion MR imaging--pilot study." Radiology **249**(3): 891-899.

Lyng, H., O. Haraldseth and E. K. Rofstad (2000). "Measurement of cell density and necrotic fraction in human melanoma xenografts by diffusion weighted magnetic resonance imaging." Magn Reson Med **43**(6): 828-836.

McConnell, J. F., L. Garosi and S. R. Platt (2005). "Magnetic resonance imaging findings of presumed cerebellar cerebrovascular accident in twelve dogs." Vet Radiol Ultrasound **46**(1): 1-10.

Mehan, W. A., Jr., R. G. Gonzalez, B. R. Buchbinder, J. W. Chen, W. A. Copen, R. Gupta, J. A. Hirsch, G. J. Hunter, S. Hunter, J. M. Johnson, H. R. Kelly, M. Larvie, M. H. Lev, S. R. Pomerantz, O. Rapalino, S. Rincon, J. M. Romero, P. W. Schaefer and V. Shah (2014). "Optimal brain MRI protocol for new neurological complaint." PLoS One **9**(10): e110803.

Merboldt, K. D., H. Bruhn, J. Frahm, M. L. Gyngell, W. Hanicke and M. Deimling (1989). "MRI of "diffusion" in the human brain: new results using a modified CE-FAST sequence." Magn Reson Med **9**(3): 423-429.

Moffat, B. A., T. L. Chenevert, T. S. Lawrence, C. R. Meyer, T. D. Johnson, Q. Dong, C. Tsien, S. Mukherji, D. J. Quint, S. S. Gebarski, P. L. Robertson, L. R. Junck, A. Rehemtulla and B. D. Ross (2005). "Functional diffusion map: a noninvasive MRI biomarker for early stratification of clinical brain tumor response." Proc Natl Acad Sci U S A **102**(15): 5524-5529.

Moseley, M. E., Y. Cohen, J. Mintorovitch, L. Chileuitt, H. Shimizu, J. Kucharczyk, M. F. Wendland and P. R. Weinstein (1990). "Early detection of regional cerebral ischemia in cats: comparison of diffusion- and T2-weighted MRI and spectroscopy." Magn Reson Med **14**(2): 330-346.

Muller, M. F., P. Prasad, B. Siewert, M. A. Nissenbaum, V. Raptopoulos and R. R. Edelman (1994). "Abdominal diffusion mapping with use of a whole-body echo-planar system." Radiology **190**(2): 475-478.

Namimoto, T., Y. Yamashita, K. Mitsuzaki, Y. Nakayama, Y. Tang and M. Takahashi (1999). "Measurement of the apparent diffusion coefficient in diffuse renal disease by diffusion-weighted echo-planar MR imaging." J Magn Reson Imaging **9**(6): 832-837.

Namimoto, T., Y. Yamashita, S. Sumi, Y. Tang and M. Takahashi (1997). "Focal liver masses: characterization with diffusion-weighted echo-planar MR imaging." Radiology **204**(3): 739-744.

Neil, J. J. (1997). "Measurement of Water Motion (Apparent Diffusion) in Biological Systems ." Concepts in Magnetic Resonance **9**(6): 385-401.

Nemanic, S., K. Hollars, N. C. Nelson and G. Bobe (2015). "Combination of Computed Tomographic Imaging Characteristics of Medial Retropharyngeal Lymph Nodes and Nasal Passages Aids Discrimination between Rhinitis and Neoplasia in Cats." Vet Radiol Ultrasound.

Nyman, H. T., A. T. Kristensen, I. M. Skovgaard and F. J. McEvoy (2005). "Characterization of normal and abnormal canine superficial lymph nodes using gray-scale B-mode, color flow mapping, power, and spectral Doppler ultrasonography: a multivariate study." Vet Radiol Ultrasound **46**(5): 404-410.

Nyman, H. T. and R. T. O'Brien (2007). "The sonographic evaluation of lymph nodes." Clin Tech Small Anim Pract **22**(3): 128-137.

Owen, L. (1980). TNM Classification of Tumours in Domestic Animals. Geneva, World Health Organization.

Padhani, A. R., G. Liu, D. M. Koh, T. L. Chenevert, H. C. Thoeny, T. Takahara, A. Dzik-Jurasz, B. D. Ross, M. Van Cauteren, D. Collins, D. A. Hammoud, G. J. Rustin, B. Taouli and P. L. Choyke (2009). "Diffusion-weighted magnetic resonance imaging as a cancer biomarker: consensus and recommendations." Neoplasia **11**(2): 102-125.

Park, S. O., J. K. Kim, K. A. Kim, B. W. Park, N. Kim, G. Cho, H. J. Choi and K. S. Cho (2009). "Relative apparent diffusion coefficient: determination of reference site and validation of benefit for detecting metastatic lymph nodes in uterine cervical cancer." J Magn Reson Imaging **29**(2): 383-390.

Pokorny, E., S. Hecht, P. A. Sura, A. K. LeBlanc, J. Phillips, G. A. Conklin, K. A. Haifley and K. Newkirk (2012). "Magnetic resonance imaging of canine mast cell tumors." Vet Radiol Ultrasound **53**(2): 167-173.

Roberts, T. P. L. and R. H. A. (2003). "Diffusion weighted magnetic resonance imaging in stroke." European Journal of Radiology **45**: 185-194.

Roy, C., G. Bierry, A. Matau, G. Bazille and R. Pasquali (2010). "Value of diffusion-weighted imaging to detect small malignant pelvic lymph nodes at 3 T." Eur Radiol **20**(8): 1803-1811.

Salwei, R. M., R. T. O'Brien and J. S. Matheson (2005). "Characterization of lymphomatous lymph nodes in dogs using contrast harmonic and Power Doppler ultrasound." Vet Radiol Ultrasound **46**(5): 411-416.

Sasaki, M., K. Yamada, Y. Watanabe, M. Matsui, M. Ida, S. Fujiwara, E. Shibata and I. Acute Stroke Imaging Standardization Group-Japan (2008). "Variability in absolute apparent diffusion coefficient values across different platforms may be substantial: a multivendor, multi-institutional comparison study." Radiology **249**(2): 624-630.

Shimony, J. S., R. C. McKinstry, E. Akbudak, J. A. Aronovitz, A. Z. Snyder, N. F. Lori, T. S. Cull and T. E. Conturo (1999). "Quantitative diffusion-tensor anisotropy brain MR imaging: normative human data and anatomic analysis." Radiology **212**(3): 770-784.

Smith, M. M. (1995). "Surgical Approach for lymph node staging or oral and maxillofacial neoplasms in dogs." Journal of the American Animal Hospital Association **31**(6): 514-518.

Srinivasan, A., R. Dvorak, K. Perni, S. Rohrer and S. K. Mukherji (2008). "Differentiation of benign and malignant pathology in the head and neck using 3T apparent diffusion coefficient values: early experience." AJNR Am J Neuroradiol **29**(1): 40-44.

Stejskal, E. O., Tanner, J.E. (1965). "Spin diffusion measurements: spin echoes in the presence of a time-dependent field gradient." J Chem Phys **42**: 288-292.

Studer, H. C. T. J. M. F. M. T. J. H. L. J. B. P. V. A. F. U. E. (2014). "Metastases in Normal-sized Pelvic Lymph Nodes: Detection with DIffusion-weighted MR Imaging." **273**(1): 125-135.

Sumi, M., S. Noriyuki, S. Tadateru, M. Minoru, U. Masataka, K. Hiroyuki, S. Koichiro, H. Kuniaki, T. Haruo and N. Takashi (2003). "Discrimination of Metastatic Cervical Lymph Nodes with Diffusion-Weighted MR Imaging in Patients with Head and Neck Cancer." AJNR Am J Neuroradiol **24**: 1627-1634.

Sutherland-Smith, J., R. King, D. Faissler, R. Ruthazer and A. Sato (2011). "Magnetic resonance imaging apparent diffusion coefficients for histologically confirmed intracranial lesions in dogs." Vet Radiol Ultrasound **52**(2): 142-148.

Szafer, A., J. Zhong and J. C. Gore (1995). "Theoretical model for water diffusion in tissues." Magn Reson Med **33**(5): 697-712.

Szakall, S., Jr., O. Esik, G. Bajzik, I. Repa, G. Dabasi, I. Sinkovics, P. Agoston and L. Tron (2002). "18F-FDG PET detection of lymph node metastases in medullary thyroid carcinoma." J Nucl Med **43**(1): 66-71.

Takahara, T. (2005). "DWIBS: Diffusion-weighted whle-body imaging with background body signal suppression." Medica Mundi **49**(3): 38-41.

Takahara, T., I. Yutaka, Y. Tomohiro, Y. Seiei, N. Seiji and V. C. Marc (2004). "Diffusion Weighted Whole Body Imaging with Background Body Signal Suppression (DWIBS): Technical Improvement Using Free Breathing, STIR and High Resolution 3D Display." Radiation Medicine **22**(4): 275-282.

Thoeny, H. C., F. De Keyzer, F. G. Claus, S. Sunaert and R. Hermans (2005). "Gustatory stimulation changes the apparent diffusion coefficient of salivary glands: initial experience." Radiology **235**(2): 629-634.

Thoeny, H. C., F. De Keyzer, V. Vandecaveye, F. Chen, X. Sun, H. Bosmans, R. Hermans, E. K. Verbeken, C. Boesch, G. Marchal, W. Landuyt and Y. Ni (2005). "Effect of vascular targeting agent in rat tumor model: dynamic contrast-enhanced versus diffusion-weighted MR imaging." Radiology **237**(2): 492-499.

Turner, R., D. Le Bihan, J. Maier, R. Vavrek, L. K. Hedges and J. Pekar (1990). "Echo-planar imaging of intravoxel incoherent motion." Radiology **177**(2): 407-414.

Vexler, V. S., Roberts, T.P., Rosenau, W. (1996). "Early detection of acute tubular injury with diffusion-weighted magnetic resonance imaging in a rat model of myohemoglobinuric acute renal failure." Ren Fail **18**: 41-57.

Vos, J. H., T. S. van den Ingh and F. N. van Mil (1989). "Non-exfoliative canine cytology: the value of fine needle aspiration and scraping cytology." Vet Q **11**(4): 222-231.

Walker, L., L. C. Chang, A. Nayak, M. O. Irfanoglu, K. N. Botteron, J. McCracken, R. C. McKinstry, M. J. Rivkin, D. J. Wang, J. Rumsey, C. Pierpaoli and G. Brain Development Cooperative (2016). "The diffusion tensor imaging (DTI) component of the NIH MRI study of normal brain development (PedsDTI)." Neuroimage **124**(Pt B): 1125-1130.

Wan, C. W., C. Y. Lee, C. Y. Lui, C. Y. Fong and K. C. Lau (2016). "Apparent diffusion coefficient in differentiation between malignant and benign breast masses: does size matter?" Clin Radiol **71**(2): 170-177.

Wang, J., Q. Liao, Y. Zhang, C. Yu, R. Bai and H. Sun (2012). "Differential diagnosis of axillary inflammatory and metastatic lymph nodes in rabbit models by using diffusion-weighted imaging: compared with conventional magnetic resonance imaging." Korean J Radiol **13**(4): 458-466.

Wang, J., S. Takashima, F. Takayama, S. Kawakami, A. Saito, T. Matsushita, M. Momose and T. Ishiyama (2001). "Head and neck lesions: characterization with diffusion-weighted echo-planar MR imaging." Radiology **220**(3): 621-630.

Westbrook, C., Roth, C.K., Talbot, J. (2011). Functional imaging techniques, In: MRI in Practice. Chichester, West Sussex, Wiley-Blackwell.

Westbrook, C., Roth, C.K., Talbot, J. (2011). Pulse sequences, In: MRI in Practice. Chichester, West Sussex, Wiley-Blackwell.

Williams, L. E. and R. A. Packer (2003). "Association between lymph node size and metastasis in dogs with oral malignant melanoma: 100 cases (1987-2001)." J Am Vet Med Assoc **222**(9): 1234-1236.

Wu, L.-M., J.-R. Xu, J. Hua, H.-Y. Gu, J. Zhu and J. Hu (2013). "Value of Diffusion-Weighted MR Imaging Performed with Quantitative Apparent Diffusion Coefficient Values for Cervical Lymphadenopathy." Journal of Magnetic Resonance Imaging **38**
: 663-670.

Wu, L. M., J. R. Xu, J. Hua, H. Y. Gu, J. Zhu and J. Hu (2013). "Value of diffusion-weighted MR imaging performed with quantitative apparent diffusion coefficient values for cervical lymphadenopathy." J Magn Reson Imaging **38**(3): 663-670.

APPENDIX A: Equations

Equation 1: $b = \gamma^2 \; G_i^2 \; \delta^2 \; (\Delta - \delta/3)$

> γ = gyromagnetic ratio, G_i = strength of the gradient, δ = length of time for which the gradients are turned on, and Δ = time interval between the gradient pulses

Equation 2: $ADC = (1/\; b_1 - b_0) \; \ln(S[b_0]/S[b_1])$

> b_1 and b_0 are the b-values used, $S[b_1]$ is the signal intensity acquired with b-value b_1, and $S[b_0]$ is the signal intensity acquired with b-value b_0

Equation 3: $S_b / S_0 = (1\text{-}f) \exp(\text{-}bD) + (f) \exp(\text{-}bD^*)$

> S is the mean signal intensity, f is the fraction of the diffusion due to microcirculation, D is the true diffusion coefficient, and D* is the pseudodiffusion coefficient

APPENDIX B: Tables

Table 1: Characterization of Evaluated Lymph Nodes

Lymph Node Characterization	Number of Metastatic Lymph Nodes	Number of Benign Lymph Nodes	Total Number of Lymph Nodes
Enlarged	6	4	10
Non-Enlarged	-	10	10
Total Number of Lymph Nodes	6	14	20

Table 2: Qualitative DWI and ADC Appearance of Enlarged Lymph Nodes

Subject	DWI Appearance	ADC Appearance	Characterization
A	Iso- to hyperintense	Isointense	Metastatic
B	Iso- to hyperintense	Isointense	Benign
C	Hypointense	Hypointense	Metastatic
D	Isointense	Iso- to hypointense	Metastatic
E1	Hyperintense	Iso- to hyperintense	Benign
E2	Iso to hyperintense	Iso- to hyperintense	Benign
F1	Isointense	Isointense	Metastatic
F2	Isointense	Isointense	Metastatic
G	Hyperintense	Iso- to hyperintense	Metastatic
H	Hyperintense	Isointense	Benign

*Intensity is relative to the mandibular salivary glands

Table 3: Inter-observer Coefficient of Variation (CV)

	CV	Lower Limit	Upper Limit
Benign	10.39	1.96	18.81
Metastatic	15.88	6.98	24.77

*Acceptable CV level is 10%

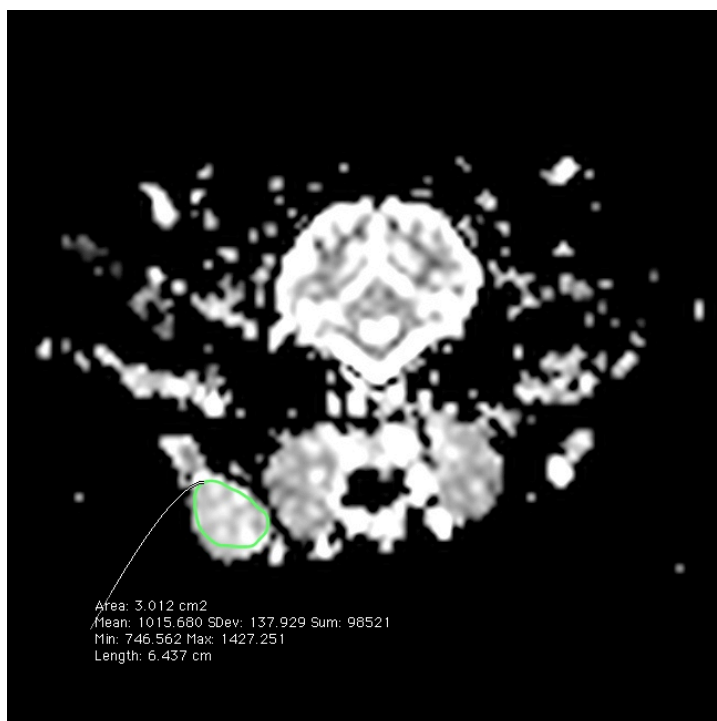**Table 4:** Accuracy of Pooled Observer Subjective Lymph Node Assessment vs. Pathologist Characterization (True)

Subjective assessment based on MR appearance	Lymph node pathologic assessment (true characterization)		
	Benign (B)	Metastatic (M)	Total
Benign (B)	33	8	41
Metastatic (M)	4	8	12
M/ B	5	2	7
Total	42	18	60

Figure 1: ROIs on T2-Weighted and ADC Sequences

A. T2-weighted image ROI surrounding an enlarged right mandibular lymph node.

B. ADC map image with the ROI from the T2-weighted image copied and pasted.

Figure 2:
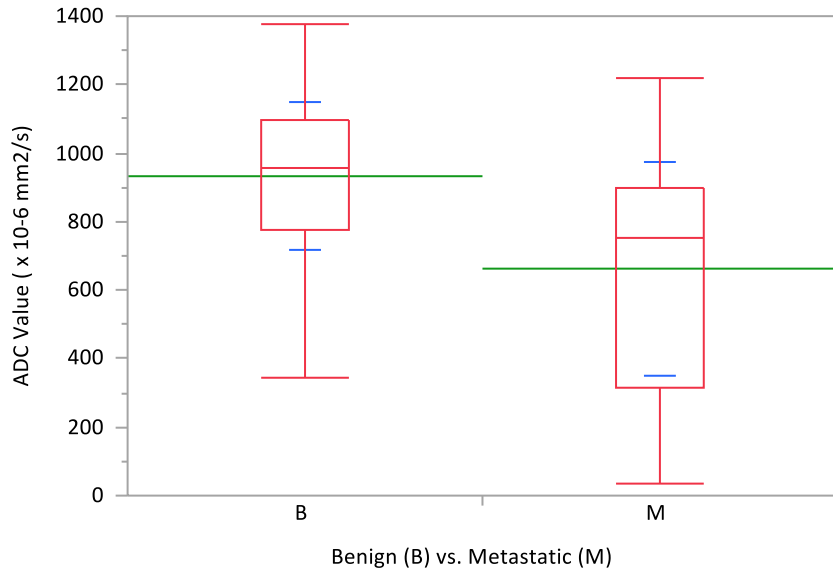
ADC Values of All Benign vs. Metastatic Lymph Nodes
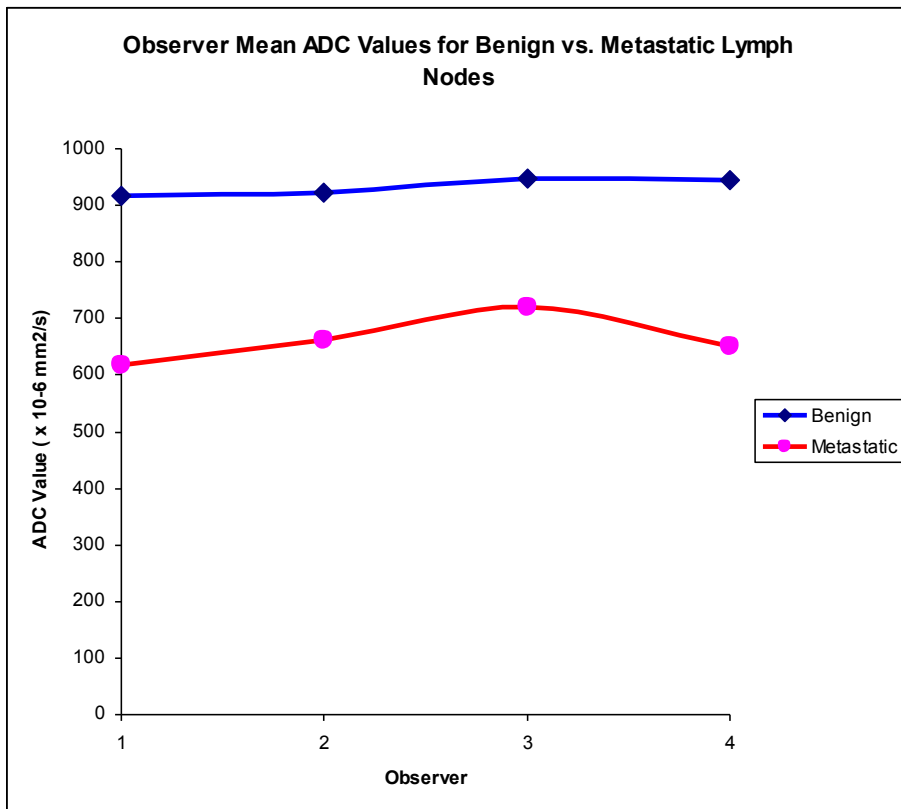

Figure 3:

Figure 4:

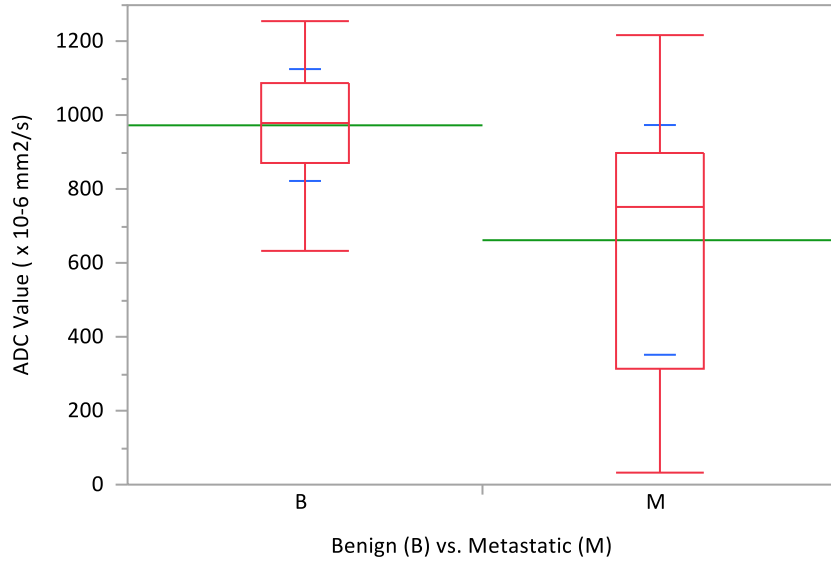**ADC Values of Enlarged Benign and Metastatic Lymph Nodes**

Figure 5: